ADVANCED ENERGY MATERIALS
www.advenergymat.de

Design Strategies for Practical Zinc-Air Batteries Toward Electric Vehicles and beyond

*Sambhaji S. Shinde, Sung-Hae Kim, Nayantara K. Wagh, and Jung-Ho Lee**

Zinc-air batteries (ZABs) offer promising forthcoming large-scale high-density storage systems and the cost-effectiveness of electrode materials, specifically in solid-state and liquid electrolytes. However, the uncontrolled diffusion and utilization of irreversible zinc components and cell design principles limit practical applications with severe capacity fade and interfacial reactions. In this perspective article, the aim is to shed lights on the underlying mechanisms of solid electrolytes and interfaces alongside the current status and prospective research insights. Formulations of ampere-hour (Ah)-scale cylindrical/pouch cells are discussed for 100–500 Wh kg^{-1} cell-level energy metrics under realistic operations. The electrode/electrolyte interface dynamics, scale-up readiness, testing protocols, and key performance metrics are also suggested for transforming lab-scale research into practical production.

1. Why are Zinc-Air Batteries Among Metal-Air Batteries?

By 2030, the global battery demands are projected to be 4500–4700 GWh, ≈8 times the market in 2020 (**Figure** 1a); however, lithium-ion batteries (LIBs) forecast 1200–1600 GWh due to limited lithium (Li), nickel (Ni), and cobalt (Co) reserves. Thus, battery chemistries with earth-abundant metals are critically desirable.[1] Metals such as zinc (Zn), magnesium (Mg), aluminum (Al), calcium (Ca), sodium (Na), iron (Fe), silicon (Si), and potassium (K) have revival interests owing to increasing anxieties for global energy security. Theoretical energy densities of metal-air batteries (MABs) range from 935 to 5200 Wh kg^{-1}(including oxygen) and 1350-11200 Wh kg^{-1} (excluding oxygen). MABs market projects 500–900 GWh (≈10%–20% out of the total market share) by 2030 in various applications (Figure 1b).[2] Particularly, EVs market demands cell-level specific-energy of >500 Wh kg^{-1}, volumetric-energy (E_{vol} >1500 Wh L^{-1}), and ~75 US$ kWh^{-1}. Zn-air batteries (ZABs) are one of the most promising alternatives to LIBs owing to the practical specific energy of 500–600 Wh $kg^{-1}{}_{cell}$, E_{vol} of 1000–2000 Wh L^{-1}, and power (>1000 W kg^{-1}) with a driving range of 800–2000 km, cost-effective, eco-friendliness, and high safety. Commercial EVs (e.g., Tesla, Hyundai, Kia, BMW, Audi, Polstar, Chevrolet) present a driving range of 120–500 km with specific energies of 120–250 Wh $kg^{-1}{}_{cell}$ (Figure 1c), compared to 10–100 Wh $kg^{-1}{}_{cell}$ of other MABs reported to date (M = Li, Na, K, Mg, Al, Fe, Ca, Si, Table S1, Supporting Information).[3] Besides, the Li, Na, and K anodes are unsatisfactory for chemical stability and environmental safety. In contrast, the Mg, Al, Ca, Si, and Fe anodes are irreversible during charge-discharge and have lower reduction potentials, thus causing poor Coulombic efficiency and serious self-discharge phenomena. So far, due to limited material resources presented for electrodes and electrolytes, other MABs are in the early stages of development. The exponential growth of EVs by 2030 requires 4–5 times higher specific and volumetric energy densities, operations over wide temperatures, and fast charging (≈5 min) with a pack cost of <10000 USD to replace gasoline-powered vehicles. However, present high-performance EVs (Tesla) take ≈15 min for a 320 km driving range at supercharge stations. ZABs effectively promote recycling and resource recovery with green environmental impacts compared to LIBs and others (Figure 1d).

Some startup companies [i.e., e-Zinc (Canada), Phinergy (Italy), ZnR Batteries (France), Flexolyte (Korea), ZAF Energy Systems, REVEO, Inc., AMERICAN ENERGY, Eos Energy Storage, LINCDYNE, and QuantumSphere (USA)] have projected development strategies for mass production of ZABs in the upcoming few years (2028–2030). Most startups assemble the liquid coin or prototypes with Zn anode, potassium hydroxide (KOH) electrolyte, and carbon with atmospheric oxygen as cathodes; however, optimal electrode materials are yet to be determined. Very recently, a series of commercially valuable electrode materials (CuP_xS_y cathodes, CBCs electrolytes, and preferential Zn

S. S. Shinde, S.-H. Kim, N. K. Wagh, J.-H. Lee
Department of Materials Science and Chemical Engineering
Hanyang University
Ansan, Gyeonggi-do 15588, South Korea
E-mail: jungho@hanyang.ac.kr
S. S. Shinde, N. K. Wagh, J.-H. Lee
LINCDYNE Inc.
Towson, MD 21204, USA
S. S. Shinde, N. K. Wagh, J.-H. Lee
Flexolyte Inc.
Ansan, Gyeonggi 15588, South Korea

The ORCID identification number(s) for the author(s) of this article can be found under https://doi.org/10.1002/aenm.202405326

DOI: 10.1002/aenm.202405326

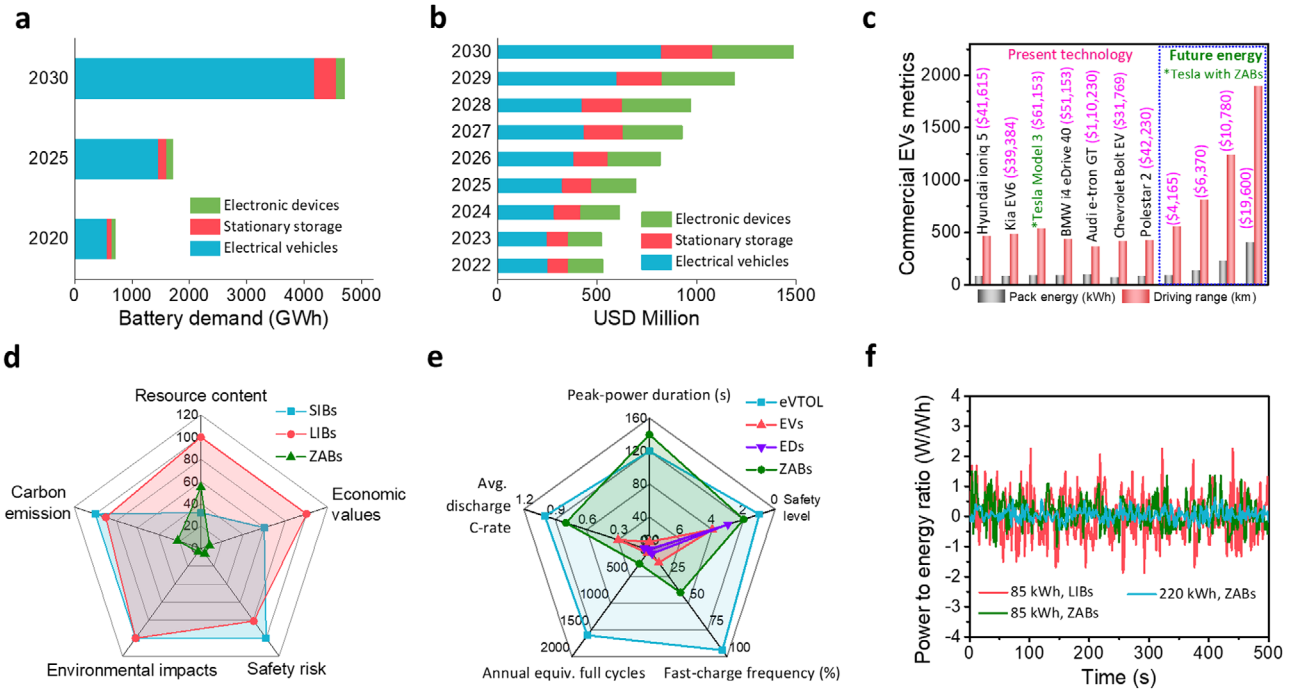

Figure 1. The state-of-the-art battery energy metrics and the present industrial scenario for electric vehicles and other applications. a) The proposed battery demand in GWh for electronic devices (EDs), stationary storage (SS), and electric vehicles (EVs) up to the year 2030. b) The predicted metal-air battery demands (USD Million) by 2030. c) Cell-pack energy and driving range of commercial EVs (left) and the future energy (right) showing projected driving range with Tesla Model 3 Long range using ZABs pack-energies of 85, 130, 220, and 400 kWh.[3a,c] d) Ragone plots for the carbon emissions, environmental impacts, safety risks, economic values, and resource contents for using 1 kg of Na-ion, Li-ion, and Zn-air batteries. The safety risk is estimated for EUCAR standards. EUCAR is the European Council for Automotive R&D. e) Storage technology requirements for EDs, EVs, and (eVTOLs) and obtained ZABs performance metrics. f) Calculated power-to-energy ratio for 85 and 220 kWh for LIBs and ZABs using vehicle dynamics model with Urban Dynamometer Driving Schedule (UDDS) driving cycles.[4] Please see methods for details.

anodes) has been developed to fabricate solid-state cylindrical and pouch-type Zn-air cells with 1–10 Ah capacity (specific energy >100-450 Wh kg^{-1}). Solid-state ZABs are potential technologies for expecting simultaneous high power-energy characteristics and fast-charge capabilities owing to bipolar stacking and using processed Zn-anodes and solid-electrolytes (SEs) to prevent unwanted chemical interactions with high device safety. Developing advanced electrode materials with exceptional kinetics, interface compatibility, and assembling practical full-ZABs are of paramount importance to commercialize ZABs. This article aims at the modern transitions of ZABs for realistic large-scale production and envisions the path forward.

2. Future Battery Demands for EVs, EDs, and eVTOL

Figure 1e compares the battery parameters required for EVs, EDs, and electric vertical takeoff and landing aircrafts (eVTOL) applications. The power profiles (Figure 1f) for ZABs simulate the C-rates (0.7-1C) higher than Tesla model-3 LIBs (0.3C) using the vehicle dynamics model. EV and ED batteries operate at lower C-rates (C/3 and C/20) specific energy than those of eVTOL (>1C).[4] Due to takeoff and landing, eVTOL requires high peak power for longer timescale of 30–120 s than EVs (10–20s) and EDs (≈1 s). Fast-charging frequency and utilization rates require 55, 10, and 1600 full-cycles per year for EVs, EDs, and eVTOL operations, respectively. European Council for Automotive R&D (EUCAR) safety standards for EVs, EDs, and eVTOL are level 4, 3, and 1, respectively, and charging time of ≈5–10 min. Heat generation for EVs is 10–100 times lower than eVTOL and EDs. Solid ZABs can display benchmark parameters of C-rate (0.8–1C), peak-power timescale (110–140 s), safety level 1–2, and fast-charge frequencies of 260 full-cycles, which are 5–10 times higher than the specifications required for EVs (Table S2, Supporting Information).[3]

3. The Need for All-Solid Zinc-Air Batteries

ZABs with aqueous/non-aqueous electrolytes facilitate fast ion transport across solid-liquid electrodes; however, Zn irreversibility, dendritic growth, volume changes, rapid consumption/high-reactivity of electrolyte with Zn forming "dead Zn", poor Coulombic efficiencies (CEs), and catastrophic-failure are the major limitations. Superior SEs can offer promising advantages such as thermodynamic stability with Zn, diminishing O_2 and H_2O crossovers, alleviating Zn-dendrites, and catalysts dissolution. Therefore, high Zn plate/strip reversibility or charge/discharge under high current density with in-planar morphology and suppressing hydrogen evolution illustrate valuable insights for mass transport and capacity limitations. In addition, solid-state ZABs contain laminated stacks of composite cathodes, SEs, and Zn-anodes. Bipolar stacks with

high-capacity cathodes/anodes increase the voltage/capacity of cells in series/parallel connections due to a reduced number of gas-diffusion-layer (GDL), Zn-anodes, and individual packaging, which decreases the weight and volume of cells, thereby increasing energy densities. The proper function of active composite materials is critical to realize solid ZABs. Since oxidation-reduction reactions cause small volume changes during cycling, generating local stress/strain among the electrodes, cell pressure is vital for optimizing solid ZABs.

4. Design Strategies for Cathodes

Emerging materials are often characterized as metal-oxides/chalcogenides, M-N or ZIF-based, and metal-free catalysts, and their properties are strongly influenced by ion/electron-interactions redox reactions (**Figure** 2a,b; Table S3, Supporting Information). Transition-metals (TMs)-based catalysts have been primarily overlooked with the lowest ORR/OER bifunctional performance of 0.56 V; however, recent work suggests that controlled ion interactions (anions, alkali/transition metals) can enhance the activities for proton-coupled electron transfer reactions by breaking pH-dependency among the active sites and reactions-of-interest. Electrocatalytic activities occur by triple-phase interphases of electrolytes, cathodes, and oxygen with key mechanisms such as phase-structures, sequential electrochemical-chemical (E–C′), electronic properties (energy barriers, and charge/mass transfer), and co-catalysts/ion-shuttling (Figure 2c). Ion interactions cause structural transitions from the atomic-to-mesoscale due to mechanical strain and increase the van der Waals spacing, improving the electrochemically active surface area and overall catalytic activities. Upon electrochemical cycling, the repetitive ion insertion/removal leads to structural degradation or amorphization of catalysts, forming metastable structures.

For E–C′ kinetics, the electrochemical step (E) first transfers electrons in/out of the external circuit and couples with interacted-ions of electrocatalysts in the electrolytes. Then, the chemical step (C′) follows the coupled ion-electron transfer of secondary electrocatalyst phases to reactants in the electrolytes without net transfer of electrons in/out of the external circuit and reforms the electrocatalyst phase before the E step. For E > C′-rates, the E generates active phases more rapidly than consumption due to limited solid-state ion transport in the electrodes. For C′ > E-rates, the reaction follows simply electron transfer without chemical steps over the electrocatalyst phase before E ion-coupled reactions. Typically, the E–C′ kinetics occurs if catalysts act as hosts for intermediate reactants in catalyst reactions. In MnO_2-catalysts, both protons/electrons transfer between O_2 and MnO_2 through electrolyte-electrode interfaces.

Electronic structure modulates electrocatalysts' active-sites electron filling and carrier density by converting more active oxidation states, resulting in electrically conductive phases. Theoretical calculations verify that the sulfur and phosphorus active sites have (Sp–Op)*-states below the Fermi-level relative to the (Pp–Op)*-states, and electrons transfer from Cu to S-sites with partial antibonding (Sp–Op)*-states occupied for S-sites, which facilitates decent chemisorption of O* for CuP_xS_y-catalysts.[3a]

Further, anion motifs also play decisive roles in determining phase structures. The insertion of anions (O, N, S, P, Se) lowers the Fermi level in the non-bonding O-2p states, causing ligand holes, modified charge-transfer kinetics, and intermediate-binding strengths, then forming sustainable oxygen-cathodes.[3] Lower electronegativity increases the redox potential and electrical conductivity with improved n-/p-type redox kinetics. Multi-electron redox motifs offer high specific capacities. However, intrinsic sluggish kinetics originate with dual-pairs of anions (N-N, O-O, S-S, P-P, Se-Se), leading to premature capacity decay and active materials losses; thus, controlling single anion-cation pair is the desirable requirement.[3d] Coupling non-redox-active electrocatalysts with epitaxial supports substantially reduces the kinetics barriers for oxygen reactions in solid-state compared to those of liquid electrolytes (LEs); thus, it is an effective strategy for ZABs. Electrocatalytic activities have the trends for cations/anions as Cu>Fe>Mn>Co>Ni, P>S>N>O>Se, and $Cs^+>Rb^+>K^+>Na^+>Li^+$.

The reversibility for ORR/OER processes is the major concern for improving ZABs cycling under solid-electrolytes. Previous reports state the influence of H_2O for ORR/OER directly affects the Zn dissolving/deposition processes in ZABs with poor wettability for cathodes. The high viscosity of SEs illustrates the severe potential drops for ZABs owing to low wettability with gas-diffusion electrodes. Besides, the existing smaller metal cations originate the irretrievable drop of O_2 gases, implying the formation of insoluble metal peroxides or superoxides as strong nucleophiles by one-electron transfer with a negative impact over the ORR kinetics. In contrast, larger cations contribute to the reversible O_2/O_2^- reactions. Mechanisms for how reactive superoxides can maintain stability for re-oxidation back to O_2 upon ZAB operations are still in their infancy. These stabilized superoxide radicals re-oxidize during reversible potential sweeps rather than reacting to other molecules owing to ion-pairing interactions. However, CEs are critically reduced because of the dissimilarity in diffusivity between the superoxide radicals and O_2 gas. Further, the energy barriers at the electronic structures level for ORR/OER reactions are as follows: 1) The higher oxygen dissociation barriers or adsorption energies generate the more positive d-band centers; 2) The hydrostatic compressive stress severely increases the lattice constants by generating lattice strains, decreasing d-band width; 3) The formation energy increases more positively along with segregation energy; 4) The destruction of electronic structures critically decrease the electrical conductivity of cathodes because of the redistribution of inter-element valence electrons; 5) substantial inflection in the work function of catalysts during water dissociation reactions for constant charge or discharge conditions. For anodes, the larger nucleation overpotentials reduce mass/charge transfer, desolvation, and electrocrystallization (nucleation and growth), growth morphological instabilities and dead Zn or dendrites are the additional challenges.

5. Design Strategies for Electrolytes

Electrolytes play a critical role for ZABs because their chemical structures openly influence electrochemical reactions and diffusion kinetics of cations/anions. SEs are categorized as solid-polymer-electrolyte (SPE), anion-exchange-membrane (AEM), and hydrogel/gel-polymer-electrolyte (GPE). SPEs show the lowest conductivity (<1 mS cm^{-1}), but GPE has the highest conductivity (100–300 mS cm^{-1}); however, the poor

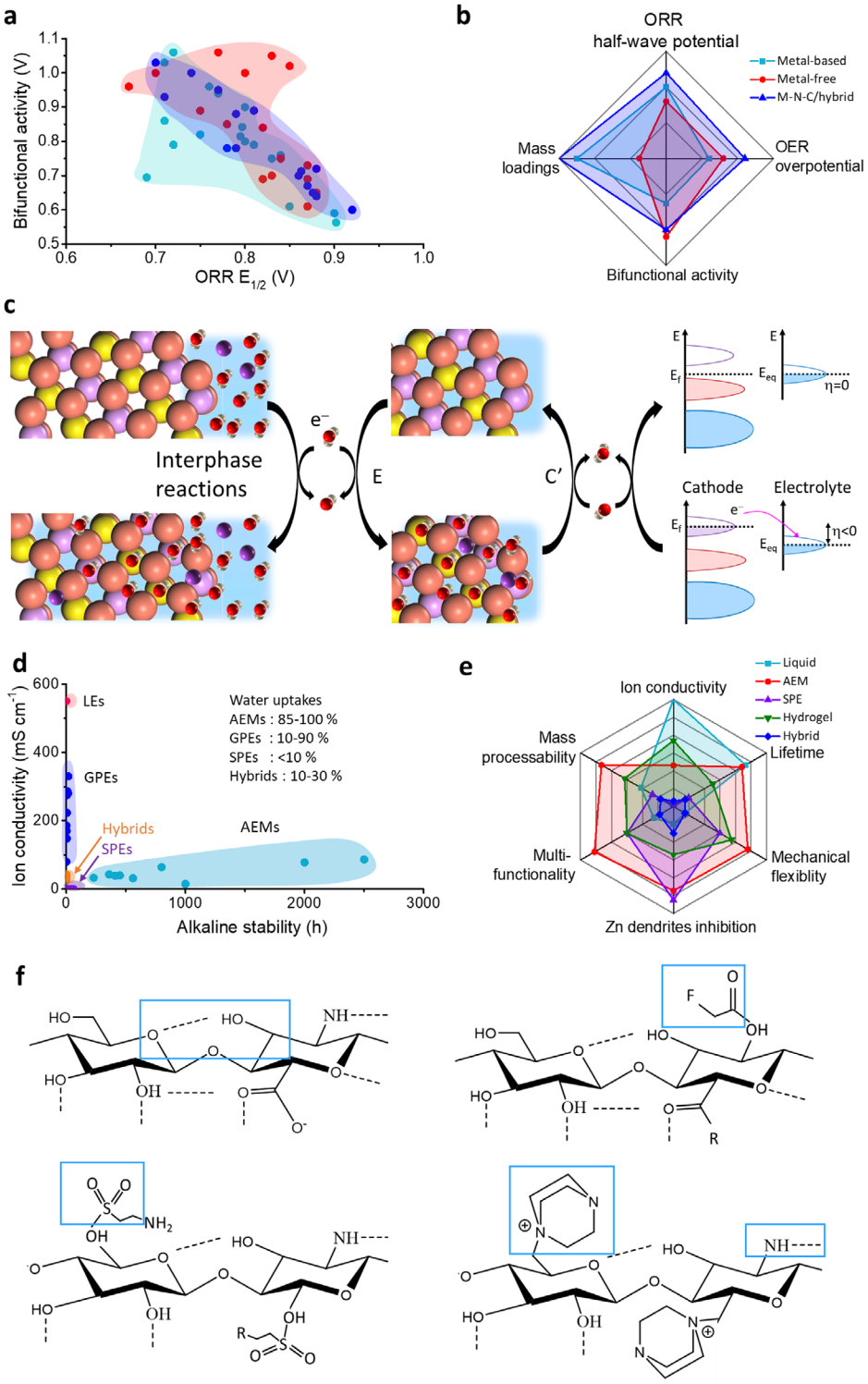

Figure 2. Mechanistic illustrations for designing high-performance cathode and solid electrolytes. a) Comparison of bifunctional activity versus ORR half-wave potentials. b) Radar charts grading the performance metrics for bifunctional catalysts. c) Structural influences for active electrochemical surface areas beyond the electrode-electrolyte interphases (left). Electrochemical-chemical kinetics (E-C') with insertion of intermediate reactants by transferring both the electrons and ions across the interface (middle). Kinetics for distribution of electrons for catalysts structure (right). The thermodynamic-electrochemical driving force and electrical conductivity depend significantly on the position of the Fermi level. d) Comparison of the anion-exchange membranes (AEMs), gel-polymer electrolytes (GPEs), and solid-polymer electrolytes (SPEs) based on the recently reported champion data. e) Radar chart for electrolyte performance metrics. f) Anion-motifs-related structures for SEs. TEMPO and O-motifs (top, left), F -motif (top, right), S-motif (bottom, left), quaternary and N-motifs (bottom, right).

Table 1. Comparison of the reported high-performance solid-state electrolytes for Zn-air batteries.

Electrolyte type	Electrolyte	Ion conductivity [mS cm^{-1}]	Water uptake [%, RT]	Alkaline stability [°C/h]	Manufacturing feasibility/flexibility	Interface functionality	Thermal stability	Refs.
Anion-exchange membranes (AEMs)	Chitosan biocellulosics (CBCs)	86.7	99	100/2500	Excellent	Excellent	Excellent	[3a]
	Functionalized bio-cellulose (FBN)	64	95	–	Excellent	Excellent	Excellent	[9a]
	QAFC	21.2	95	20/170	Excellent	Poor	Moderate	[10]
	A201	40	44	–	Excellent	Poor	Moderate	[11]
	QPBI	39	85	7	Moderate	Poor	Moderate	[11]
	QAFCGO	33	95	–	Moderate	Moderate	Moderate	[12]
	PVA/PDDA	25	–	80/360	Moderate	Poor	Poor	[13]
	PPO-DMHDA	35	20.4	20/75	Moderate	Poor	Poor	[14]
	AAEM	32	84	25/200	Moderate	Moderate	Moderate	[15]
	PAP-TP-85	78	46	100/2000	Moderate	Poor	Excellent	[16]
	TRP-0	15	67	60/450	Moderate	Poor	Moderate	[17]
	1.75MQAPES-OH	7.5	42	60/168	Moderate	Poor	M43oderate	[18]
	QA-PPEK-0.9	43	58.4	60/300	Moderate	Poor	Moderate	[19]
Hydrogel or Gel polymer electrolytes (GPEs)	PVA	0.13	25.6	–	Moderate	Poor	Poor	[20]
	Nano-SFQ	186	–	–	Moderate	Poor	Poor	[21]
	CCNL-PDIL	286.5	90	–	Moderate	Poor	Moderate	[22]
	P(AM-co-AA)	148	69.2	–	Excellent	Poor	Moderate	[23]
	PAM	330	–	–	Excellent	Poor	Poor	[24]
	PAM-CNF-KI	223	86	–	Excellent	Poor	Poor	[25]
	PANa-cellulose	280	–	–	Excellent	Poor	Moderate	[26]
	PVA-xTMG	80	40	–	Excellent	Poor	Poor	[27]
	A-PAA	275	60	–		Poor	Poor	[28]
	PANa	170	97.3	–	Excellentoderate	Poor	Moderate	[29]
Liquid electrolytes	1-8 M KOH	550	–	–	Excellent	Poor	Poor	[30]
	1-8 M NaOH	250	–	–	Excellent	Poor	Poor	[31]
Solid polymer electrolytes (SPEs)	PVDF, PAN, PEO, and inorganic fillers	0.001–1	–	–	Excellent	Moderate	Moderate	[32]

interface functionalities and water retention remain significant drawbacks.[5] Good ion conductivity (>90 mS cm^{-1}), lowest interface resistance, easy scale-up, multifunctionalities, and inhibition of dendrites/cathode dissolution are the major reasons why AEM plays a dominant role in solid-state ZABs development (Figure 2d,e and **Table 1**). Structural-dynamic interactions and electrochemical behavior of AEM depend on the polymeric structures, molecular weight, processing solvents, and cation-anions motifs; however, there is still a lack of deep understanding of these interactions and behavior. SEs have amorphous or partially crystalline structures, and they offer local-segmental kinetics for the migration of ions from one site to following neighboring sites under electrochemical operations. The small glass-transition temperature (T_g) based polymeric materials are the promising host for SEs owing to numerous amorphous regions, and their free-volume ensures anions/cations hopping kinetics.

Liquid electrolytes intrinsically percolate 3D porous cathodes, whereas SEs contain resistive heterogeneities; thus, percolation thresholds and particle-size distributions influence the performances. Specifically for alkaline LEs ZABs, the KOH and NaOH have good salt solubility, oxygen diffusion coefficients, and lower viscosity; however, they are disposed to evaporation or moisture absorptions. Whereas zinc trifluoromethanesulfonate ($Zn(CF_3SO_3)_2$) and zinc sulfate ($ZnSO_4$) salts are favorable for aqueous or neutral LEs, in which $Zn(CF_3SO_3)_2$ possess superior reversibility and mass/charge transfer kinetics because larger $(CF_3SO_3)_2$ anions diminish the amount of hydrated H_2O with Zn^{2+} ions. Insertion of organic or inorganic additives (lithium chloride (LiCl), zinc chloride ($ZnCl_2$), zinc fluoride (ZnF_2), Thiourea, ammonium hydroxides, propylene glycol, polyacrylamide (PAM)), amphiphilic surfactants, higher salt concentrations (2–8 M), and ionic liquids are specific strategies that encourage the proper crystal orientations and surface textures for

zinc, implying superior reversibility, stability and confined dendrites through electrostatic shielding.

GPEs consist of lower-free water, numerous functional species, and superior mechanical/thermal and self-healing characteristics that effectively mitigate the hydrogen evolution reaction (HER), corrosion, or passivation. However, the rapid loss in water retention and ion conductivity severely limits the cycle life of ZABs. Ion cross-linking of polymers (polyvinyl alcohol (PVA), PAM, polyacrylic acid (PAA), polyacrylonitrile (PAN), polyacrylic acid sodium salt (PANa) with carboxylic acids, carboxymethyl cellulose, sodium alginate, or ionic liquids (ILs) are the proper approaches that allow the construction of flexible ZABs sustaining local stresses under different mechanical deformations. Zn(II) Bis(trifluoromethanesulfonyl)imide ($Zn(TFSI)_2$) favors a unique solvation structure for Zn^{2+} that significantly inhibits the formation of hydrated zin ion complex ($(Zn\text{-}(H_2O)_6)^{2+}$) in all kinds of SEs. SPEs have nonflammable, homogeneous Zn-depositions and high mechanical characteristics that improve the practicality of Zn-anodes. However, poor ion conductivity and sluggish diffusion kinetics limit the electrochemical performances of ZABs owing to stronger electrostatic bindings for cations/anions. Utilizing ion-plasticizers, organic/inorganic fillers, and ILs are effective strategies that enhance interface compatibility. Hybrid electrolytes consist of alkali for Zn and acid for the cathode to increase the power/energy and open-circuit potential (OCP) that prevents CO_2 formation. However, charging in acids (OER) is highly unfavorable. Thus, the alkali/acid coupling of hydrogels in a bipolar membrane is one of the effective approaches. For high-energy cells, cathode mass-loading (>15 mg cm^{-2}), Zn-anode-thickness (100–300 µm), and SEs with effective ion-conductivity (>80–100 mS cm^{-1}) are realistic to achieve a specific-energy of 400–500 Wh kg^{-1}.

Figure 2f shows the interactions between coordinated structures and electrochemical ionic-transport kinetics. 1) Oxygen-containing motifs consist of carbonyl (C=O) and ether (C−O−C) interactions that enable reversible formation of radical monoanion ($C\text{-}O^-$) and cations by Coulombic attraction force and ionic-dipole interactions. 2) Sulfur-containing motifs also have similar interactions with oxygen, such as thioether (C-S-C), thiocarbonyl (C=S), and disulfide (C-S-S-C) motifs corresponding to the ether and carbonyl motifs, respectively, due to the existence in same-group of the periodic table. However, it increases the conductivity and redox potential because of the electronegativity less than oxygen. C-S-S-C has two sulfur atoms. By accepting two electrons, S-S bonds can be easily broken with the stabilization of each $R\text{-}S^-$-anion by the counter-cations. Thus, S-motif possesses multi-electron processes per motif, ensuing high ion-transport kinetics. 3) Nitrogen-containing motifs have azo (N=N), imines (C=N), nitriles (C≡N), and tertiary amines ($C-N(SO_2)-$) based on double/triple bonds of carbon and nitrogen. Tertiary amines allow higher ion mobility undergoing change-in-bond order upon reactions and electron delocalization of sulfonyl groups to nitrogen centers. Pyridinium, quaternary, or other derivatives consist of hetero-aromatic rings with N-atoms to conjugated structures that allow efficient change in molecular structures in different ways to enhance charge-transfer kinetics. 4) Fluorine-containing motifs have C-F with significant dipole moment and polarity due to high electronegativity. Electron density is focused on nearby F, ensuring highly ionic-character with partial charges ($C^{\delta+}-F^{\delta-}$). 5) The 2,2,6,6-tetra methylpiperidin-1-yl)oxyl (TEMPO) or quaternary amines contains intrinsically-bipolar N-O• nitroxide radicals that have abundant intermolecular interactions, high-solubility and self-exchange-reactions, enabling high-potential and ion-transport. This kinetics vindicates the hopping mechanism owing to segmental motion for oxygen and sulfur motifs (e.g., PVA, polyethylene oxide (PEO)), and nitrogen/fluorine/TEMPO/quaternary motifs possess both vehicle and hopping kinetics (e.g., PAM, cellulose).[6] Future efforts must focus on the structure-dynamics interactions, polarizability and binding chemistry of anionic motifs, processing conditions, multiple-compositions, and screening new materials with intrinsic ion transport with lower charge-carrier densities.

6. Design Strategies for Anodes

Figure 3a,b summarizes reported areal capacities, current rates, HER overpotential, and corrosion current/potential obtained for various types of Zn anodes (**Table 2**). The small fraction of Zn utilization per cycle (<1%) or cumulatively (30%–50%) corresponds to CEs limiting the practical viability. This conflicts with the comparative immaturity of Zn-chemistry compared to those of LIBs or LMBs; thus, it is necessary to establish harmony for commercially viable Zn-batteries target performances similar to LIBs or LMBs. Therefore, an ideal CE of 100%, plated capacity per cycle of 10 mAh cm^{-2} at 10 mA cm^{-2} (≈cumulative capacity of 10 Ah cm^{-2}) and 1000 cycles were set as a target in Figure 3a, which corresponds to 10 mAh cm^{-2} with 80% for Li passed per cycle at fast charging rates of 10 mA cm^{-2} or 2C.[7] It is clear that at least one order of magnitude performance improvement is critically required for plating/stripping current rates, Zn utilization (or depth of discharge), and areal capacity per cycle to approach a viable Zn-based battery compared to those of the present summary (Figure 3a,b and Table 2). Using interface modification strategies, Zn anode displays a plating capacity of 10 mAh cm^{-2} for 10 mA cm^{-2} with 99.8% CE limits for 200 cycles due to cell failure.[7e] Several approaches, such as epitaxial growth, crystal faceting by anions, alloying, interface modifications, and 3D structural designs, have been reported to improve the uniform nucleation or electric field distribution, corrosion kinetics, HER overpotential, areal capacity, and CEs with cycle life. The key parameters to significantly confine dendrites, by-products, and HER are optimal internal structure, surface area, and crystal orientation. Compared to previous reports, the crystal facets by anions, epitaxial growth, and interface modulation are the more competent approaches to achieve these optimal parameters.

Fast charging with minimal capacity fading needs high-capacity anodes with low redox potentials and thick cathodes. Zn-metal undergoes massive volume changes and irreversible zinc oxide (ZnO) with dendrites-growth and low Zn-utilization (<50%) upon charge-discharge. Interfacial morphological instabilities with lower Zn utilization should be overcome for reliable and safe operations of the Zn anode upon plating-stripping.[7f] Constructing diverse ion-electron conductive structures and compatible SEs with superion-transport channels is a promising strategy for high-performance Zn-anodes. The Zn trifluoromethanesulfonate and Zn bis(trifluoromethylsulfonyl)imide) additives in the electrolytes enhance the Zn reversibility; however, increased viscosity, reduced conductivity, and poor CE with

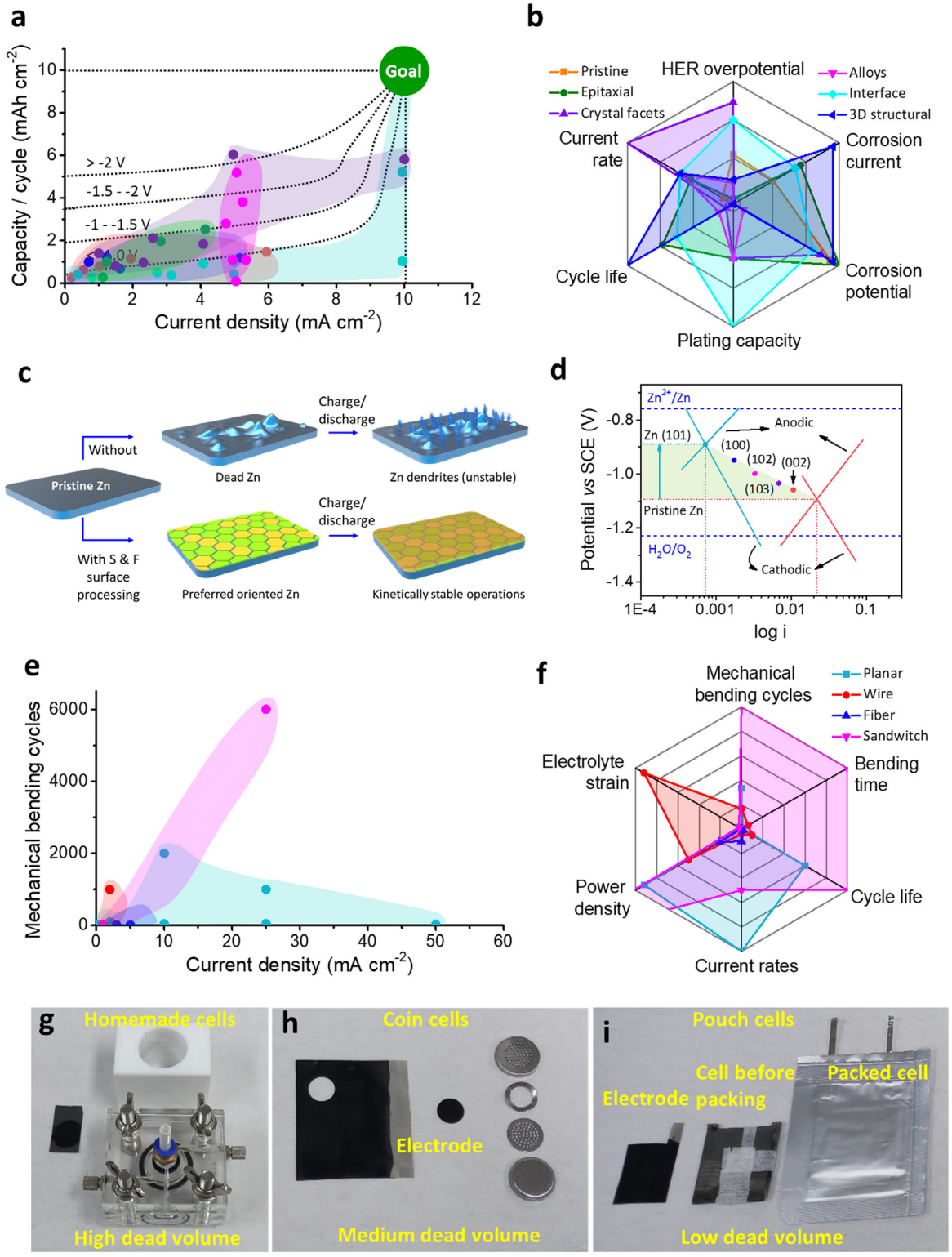

Figure 3. Illustration of designing Zn-anodes and cell performance metrics for flexible ZABs. a) Ragone plot of areal capacity versus current density for different types of Zn-anodes for symmetric cells. b) Radar chart for key performance metrics. c) Electrochemical challenges and rational design strategies for high-performance Zn-anodes with anion motifs employing the uniform current distribution, in situ formation of SEI, and anion fixation along with solid/liquid electrolytes. d) Evans diagrams for electrochemical kinetics of Zn-anodes. Reproduced with permission.[3c] Copyright 2023, Wiley. e) Comparison of mechanical bending cycles with current density for flexible ZABs for planar (cyan region), wire (red region), fiber (blue region), and sandwich(magenta region) configurations. f) Ragone plots for comparison of performance metrics in flexible ZABs. g–h) Photographs of homemade (g), coin cells (h), and pouch cells (i) and their key distinctive parameters.

Table 2. State-of-the-art for the development of various types of Zn anodes.

Zn anode types or chemistry	Anode name	HER overpotential (V)	Corrosion current (mA cm^{-2}]	Voltage hysteresis [mV]	Corrosion potential [V]	Plate/strip cycle number	CE [%]	Plating capacity [mAh cm^{-2} @mA cm^{-2}]	Zn utilization [%]	Manufacturing feasibility	Mechanical flexibility	Interface functionality	Dendrites growth	Refs.
Pristine	Zn	–	–	112	–	90	≈90	1@1	Poor	Excellent	Poor	Poor	High	[35a]
	Zn	–	0.512	105	–	100	≈90	1@1	Poor	Excellent	Poor	Poor	High	[35c]
	Zn	–		140	−1.231	30	86	1@1	Poor	Excellent	Poor	Poor	High	[36b]
	Zn	–	–	70	–	200	80	0.2@0.2	Poor	Excellent	Poor	Poor	High	[36d]
	Zn	−1.06	0.750	85	−0.975	50	83	0.25@0.5	Poor	Excellent	Poor	Poor	High	[37a]
	Zn	–	1.02	382	–	15	75	1@2	Poor	Excellent	Poor	Poor	High	[37b]
	Zn	−1.55	1.51	200	−1.06	120	76	1@6	Poor	Excellent	Poor	Poor	High	[37c]
	Zn	–	3.42	103	−0.94	135	85	1@1	Poor	Excellent	Poor	Poor	High	[37d]
	Zn	−1.175	3.41	50	−3	230	90	1@1	Poor	Excellent	Poor	Poor	High	[37e]
	Zn	–	–	56	–	30	94	1@1	Poor	Excellent	Poor	Poor	High	[37f]
	Zn	–	–	28	–	150	98	1@1	Poor	Excellent	Poor	Poor	High	[37g]
	Zn	–	2.51	73	−1.03	110	94	1@1	Poor	Excellent	Poor	Poor	High	[38c]
	Zn	–	6.63	30	−0.02 Zn	95	98	1@1	Poor	Excellent	Poor	Poor	High	[38d]
Epitaxial growth for (002) in hexagonal close-packed (hcp)	Zn(002)	−0.97	10.5	71	8.79*E-5	1000	97.7	1@1	238.18	Excellent	Moderate	Moderate	Poor	[8]
	Zn(100)	−0.86	6.1	107	7.89*E-4	200	97.7	1@1	134.83	Excellent	Poor	Poor	High	[8]
	Zn(002)	–	–	–	–	10000	99.9	1.6@40	Moderate	Excellent	Moderate	Moderate	Poor	[7f]
	Zn(002)	–	–	50	–	1600	99.1	0.25@1	Partial	Moderate	Moderate	Moderate	Poor	[8b]
	Zn(101)	–	–	59	–	200	94	0.25@1	Partial	Moderate	Moderate	Moderate	High	[8b]
	PPZ@Zn	–	2.41	86	0.032 Zn	3000	99.5	0.5@1	Moderate	Moderate	Moderate	Moderate	Moderate	[33a]
	(002)Zn	–	–	75	−1.04	600	90	2@4	Poor	Excellent	Partial	Poor	Moderate	[33b]
	(101)Zn	–	–	37	−1.045	5000	99.9	2@4	Moderate	Excellent	Partial	Moderate	Poor	[33b]
	(002)Zn	–	–	45	–	80	99.5	1@11.3	Poor	Moderate	Partial	Poor	Poor	[33c]
	Zn(002)	−2.0	3.04	66	−1.82	2000	99.6	5@5	Moderate	Moderate	Partial	Moderate	Moderate	[33d]
	Step Zn	–	–	25	–	5500	99.6	1@1	Moderate	Moderate	Moderate	Moderate	Moderate	[33e]
Crystal facet anchoring by S/F anions	Zn(101)	−2.23	–	70	−0.88	1000	99.9	5@10	Excellent	Excellent	Excellent	Excellent	Excellent	[3c]
	Zn(100)	−2.06	–	91	−0.94	1000	99.7	5@10	Excellent	Excellent	Excellent	Excellent	Excellent	[3c]
	Zn(002)	−1.74	–	186	−1.09	100	90	5@10	Partial	Excellent	Poor	Poor	Partial	[3c]
	Zn(102)	−1.99	–	141	−1.0	200	94	5@10	Moderate	Excellent	Moderate	Moderate	Moderate	[3c]
	Zn(103)	−1.82	–	214	−1.06	100	92	5@10	Moderate	Excellent	Partial	Partial	Partial	[3c]
	Bare Zn	−1.63	–	250	−1.11	325	90	5@10	Poor	Excellent	Poor	Poor	High	[3c]

(*Continued*)

Table 2. (Continued)

Zn anode types or chemistry	Anode name	HER overpotential (V)	Corrosion current (mA cm^{-2}]	Voltage hysteresis [mV]	Corrosion potential [V]	Plate/strip cycle number	CE [%]	Plating capacity [mAh cm^{-2} @mA cm^{-2}]	Zn utilization [%]	Manufacturing feasibility	Mechanical flexibility	Interface functionality	Dendrites growth	Refs.
Alloy	$ZnAg_{1-x}$	–	–	30	–	–	–	5.3@64	Poor	Moderate	Poor	Poor	Moderate	[34a]
	$Zn_{88}Al_{12}$	–	–	20	–	1000	100	5@0.5	Partial	Moderate	Poor	Poor	Moderate	[34b]
	ZnNi	−0.9722	0.589	200	−0.386	500	98	5@5	Partial	Moderate	Poor	Poor	Moderate	[34c]
	ZnBi	−1.1785	0.330	240	−0.367	100	98	5@5	Partial	Moderate	Poor	Poor	Moderate	[34c]
	GaIn@Zn	–	0.91	120	−0.965	2000	99	0.1@5	Poor	Moderate	Poor	Poor	High	[34d]
	Zn-Mn	–	–	200	–	1900	99.8	@80	Excellent	Moderate	Poor	Poor	Poor	[34e]
Interface modification						MOF/ZIF/COF based								
	ZnA@Zn	–	–	17	–	6700	99.7	1@20	Moderate	Poor	Poor	Moderate	Moderate	[35a]
	NaA@Zn	–	–	25-75	–	142	97.3	1@1	Partial	Poor	Poor	Poor	Moderate	[35a]
	Zn@ZIF8	–	0.402	70	−1.015	220	96	5@10	Partial	Poor	Poor	Poor	Moderate	[35b]
	Zn@ZIF8-5	–	–	100	–	200	97.6	10@20	Partial	Poor	Poor	Poor	Moderate	[7e]
	MOF-5W	−2.0	0.485	82	−1.176	600	~92	1@1	Partial	Poor	Poor	Poor	High	[35c]
						1D or 2D carbon based								
	CD-MWCNT	−1.157	0.330	100	−0.986	490	≈92	1@5	Partial	Poor	Poor	Poor	Moderate	[36a]
	CNTs-PT	–	0.580	30	−1.15	1300	≈98	1@1	Partial	Poor	Poor	Poor	Moderate	[36b]
	ZnNc/GO-5	–	–	–	–	–	–	–	Partial	Poor	Poor	Poor	High	[36c]
	MZn-60	–	0.45	32	–	800	–	0.2@0.2	Partial	Poor	Poor	Poor	High	[36d]
	CNTs	–	0.62	50	–	900	85	0.5@0.1	Partial	Poor	Poor	Poor	High	[36e]
						Polymers								
	PA-Zn	−1.10	0.312	105	−0.963	8000	≈99	0.25@0.5	Moderate	Excellent	Excellent	Moderate	Moderate	[37a]
	NFZP	–	0.360	57	–	900	≈99	1@2	Partial	Moderate	Poor	Poor	Poor	[37b]
	Ex-ZrP	−1.76	0.21	102	−1.03	3000	–	1@6	Moderate	Moderate	Poor	Poor	Moderate	[37c]
	P2VP	–	1.07	50	−0.84	300	95	1@1	Poor	Excellent	Excellent	Moderate	Poor	[37d]
	P4VP	–	3.16	86	−0.89	150	90	1@1	Poor	Excellent	Moderate	Moderate	Moderate	[37d]
	PS-Zn	–	2.56	123	−0.83	150	90	1@1	Poor	Excellent	Moderate	Moderate	Moderate	[37d]
	PDPTT	−1.264	2.38	75	−1.09	4200	98	1@1	Moderate	Excellent	Moderate	Moderate	Poor	[37e]
	PVDF	–	–	52	–	148	96	1@1	Poor	Moderate	Poor	Moderate	Poor	[37f]
	P-0.5%	–	–	45	–	2000	99	1@1	Moderate	Excellent	Moderate	Moderate	Moderate	[37f]
	Polymer/inorg.	–	–	75	–	200	99.8	10@10	Poor	Excellent	Moderate	Moderate	Poor	[37g]

(*Continued*)

Table 2. (Continued)

Zn anode types or chemistry	Anode name	HER overpotential (V)	Corrosion current (mA cm^{-2})	Voltage hysteresis [mV]	Corrosion potential [V]	Plate/strip cycle number	CE [%]	Plating capacity [mAh cm^{-2} @mA cm^{-2}]	Zn utilization [%]	Manufacturing feasibility	Mechanical flexibility	Interface functionality	Dendrites growth	Refs.
Metal ions or metal compounds														
	Zn@In	−1.95	–	48	–	8000	99	0.5@5	Moderate	Excellent	Excellent	Moderate	Moderate	[38a]
	ZF@F-TiO_2	–	–	24	–	450	98	1@1	Poor	Moderate	Moderate	Poor	Moderate	[38b]
	ZnSe	–	1.80	16	−1.025	1500	99.2	1@1	Partial	Poor	Poor	Poor	Moderate	[38c]
	Sn-DLC	−1.265	9.75	92	−0.01 Zn	7810	99.2	1@10	Moderate	Moderate	Moderate	Moderate	Moderate	[38d]
Structural Zn anodes	Patterned Zn	–	–	100	–	1000	99.6	1@20	Partial	Partial	Moderate	Moderate	Moderate	[3a]
	DCP-Zn	–	–	23	–	3500	99.7	0.1@0.5	Partial	Poor	Poor	Moderate	Moderate	[39a]
	N@P-Zn	–	15.1	17	−0.96	3000	96.7	1@1	Moderate	Moderate	Partial	Partial	Partial	[39b]
	3D Ti-TiO_2	–	–	51	–	2000	97.5	1@1	Partial	Poor	Partial	Partial	Partial	[39c]
	3D-Zn(002)	−1.22	–	117	–	15 000	99.8	1@5	Moderate	Moderate	Moderate	Moderate	Moderate	[39d]
	3D-Zn@C	–	0.253	32	−1.01	880	99.7	1@1	Partial	Partial	Poor	Poor	Partial	[39e]
	Zn@COF-S-F	–	0.942	34	0.033	1000	99.8	0.75@1.5	Poor	Poor	Partial	Partial	Partial	[39f]
	NP Zn	–	–	70	–	–	–	–	92	Partial	Partial	Partial	Partial	[39g]

time-dependent side reactions limit their implementations with the cost burden. The structural design and stoichiometry of Zn-based anodes significantly control effective Zn-depositions with high CEs.[7g] Thus, a fundamental understanding of interfacial reactions, surface-facet thermodynamics, and hexagonal close-packed (hcp) Zn-crystal structures upon electrochemical operations are the key strategies to determine the unique Zn-chemistries with controlled preferential crystal orientations and compositions.[3,7f,g,8] Atomic coordination, anisotropy, and dense-packing of hcp structures ensure the low-dissolution affinity relative to loosely-packed crystal facets.[8] Epitaxial growth of (002) plane maintains uniform horizontal growth of Zn microcrystals during plating. It is possible to regulate crystallization and growth of exposed Zn(002) by acid etching or sulfonate anion-induced electrodeposition methods with strong Zn^{2+} adsorption capacity of the interface to improve ion-transport kinetics, charge/mass distribution, and galvanization/exfoliation.[8b]

Two major growth kinetics for interface modifications are ex-situ and in-situ protective layers that coordinate electrolyte/electrode interfaces by promoting homogeneous nucleation and Zn growth while suppressing parasitic reactions. Design principles are chemically stable compositions in aqueous electrolytes, denser to block straight interaction among the Zn anode and electrolytes, low electronic conductivity and high Zn^{2+}-conductance confirming the Zn^{2+} deposition under the surface layer, excellent adhesion to Zn metal, and a high degree of mechanical flexibility ensuring integrity for repetitive volume changes.

The F^-/S^--treated Zn-anodes find the relevance with preferential crystal surfaces, F^-/S^- mass loadings (5–30 at%), and electrochemical-kinetics from (101), (100), (102), (103), and (002) (Figure 3c). Evans diagram reveals F^-/S^--treated Zn(101) efficiently suppresses the corrosion potential (−0.88 V closer to thermodynamic potential -0.76 V), hydrogen evolution overpotential (1.1 V), 92%–95% Zn-utilization for 5–100 mA cm^{-2}, depth-of-discharge (DOD, 60%–100%), and minimum diffusion barriers/surface energies compared to pristine Zn and Zn(100), Zn(102), Zn(103), Zn(002), manifesting high-rate capacity and dendrite-free thermo/electrochemical-stabilities (Figure 3d). Crystallographic structural orientations and electrochemical performances of Zn-anodes exhibit a favorable trend as (101)>(100)>(102)>(103)>(002). The (002) plane has a uniform charge density on a smooth surface under epitaxial growth without SEI formation but shows the poorest electrochemical performance in forming an interface with ZnS and ZnF, which stem from F^-/S^- surface treatment required for robust SEI formation.[3c,8] Zn(101) reveals 5000 and 2000 plating/stripping cycles stabilities for 5 and 10 mAh cm^{-2} capacity at 10 mA cm^{-2} with cumulative capacity (25 Ah cm^{-2}), the 2.5 times superior to Department of energy (DOE)/commercial targets. It shows a 10.2 nm ZnF_2/ZnS-rich SEI layer analogous to the SEI of viable LIBs. Similarly, Zn-alloying with Mg, Ca, Ni, copper (Cu), gold (Au), silver (Ag), mercury (Hg), molybdenum (Mo), and tin (Sn) enhances crystallographic orientations and electrochemical kinetics, whereas mechanical/chemical instabilities limit performance.

Figure 3e,f summarizes published mechanical bending cycles, current density, electrolyte stress/strain, power density, capacity, and cycle life for various cell configurations (such as planar,

wire, fiber, and sandwiched structures, **Table 3**). Mechanical tests below diffusion limiting current density (<1 mA cm^{-2}) conflict with the commercial standards for flexible Li- or other secondary batteries. To this end, it requires setting competitive targets for ZABs (1000 bending cycles for 10 mA cm^{-2} and bending time ≈100 h) comparable to Li-batteries (1000 cycles with 90% capacity retention). Previous reports validate that improvements for at least 2–3 orders of magnitude are critically required. Sandwitch-type ZABs effectively obtained the highest mechanical stability (6000 cycles for 25 mA cm^{-2}) and 95% capacity retention. This approach enables sustainable cell configurations with exceptional electrochemical performances. Planar single-layered pouch cells achieved 2000 bending cycles for 25 mA cm^{-2} with a high discharge voltage of 1.25 V.

Lab-scale experiments for ZABs utilize homemade cells with a 50–100 mAh capacity. Each application requires cells of different sizes and dimensions (prismatic, cylindrical, coin, and pouch). Pouch cells obtain maximum capacity/energy due to low package weight. For single prototype cells, stacking electrodes, air-permeable membranes, and electrolytes require less effort than winding stacks for cylindrical cells. Several stages are possible from one-to-multilayered structures and controllable active materials; however, uniform coating of cathodes for multi-stacking over porous current collectors is highly challenging. Figure 3g–i and **Table 4** compare the key distinctions, required parameters, and related challenges for transferring research outcomes from lab-scale (homemade) coins to prototype pouch cells. The internal resistance, electron transfer from welded tabs to opposite sides of each electrode, generated heat, Zn-anode thickness, and air permeation for pouch cells are the major issues required to be considered precisely for multilayered cells. Single-layer pouch cells are simple to construct but challenge establishing stable interfacial adhesion for electrolytes and other electrodes. Dead volume is also larger than multilayered cells. Processing of materials and components (i.e., mechanically stable coatings, current collectors (CCs) weldings) is also significant. Coin cells comprise the mechanical breakdown of materials, areal pressures, and their overpotentials, and they have better compatibility than pouch cells. Pressure distribution of active materials undergoes volume change in pouch cells, but it can be reformed by applying external pressures. Rational balancing mass loadings for cathodes, electrolytes, and anodes for optimal energy density and cycle life at the cell level is a significant challenge. Homemade cells utilize excess electrolyte (10–200 mL), Zn anode (10–100 g), and heavy rigid cell-case limits the practical viability of ZABs, even the researchers claiming capacity and energy density comparable to theoretical standards. The calculated capacity and energy density are just considerations of consumed Zn, which also encounters the contribution of secondary by-products. Excess amount of electrolyte (or flowing electrolyte) and anode shows several thousands of cycle life; however, the depth-of-discharge (1%–5%), state-of-charge (1%–5%), and current rates (1–5 mA cm^{-2}), which is far below the scope of commercial battery standards. To this end, the ideal testing cell configurations, such as coin or pouch cells, must be considered only. Controlling electrolyte amount, external pressure, and reduced dead volume provides substantial benefits for performance reproducibility for multilayered cells with additional complexity in process steps. In contrast, the worse control of these parameters is the major drawback of homemade and coin cells testing with limiting inference for appropriate data. **Figure 4** displays the interrelation between structural key parameters and electrochemical performances for developing cathodes, electrolytes, anodes, separators, binders, and cell design configurations for next-generation energy storage technologies.

7. Design Strategies for Solid Electrolyte Interphase (SEI)

Emerging anodes and cathodes have similar chemical/electrochemical instabilities under LEs/SEs for performance degradation (Figure S1, Supporting Information). Since the SEI-thickness severely challenges decomposition reactions for any technologies, the chemical design strategies for interfaces/interphases can alleviate it positively.[7g] Recent work utilizes electronic insulating/conducting coatings with cathode/anodes to decrease corrosion; however, it also causes chemical decomposition, voltage drops, and interdiffusions. Mechanistic understanding of coating materials, processes, and functionality for long-term stability is still lacking. Flexible SEs benefit good elastic solid-solid interface-contacts (shear modulus of separator/electrolyte > anode). Further, Zn-dendrites can be improved by SEI dominated by ZnF/ZnS as an ideal candidate for stabilizing Zn-anodes.[3,7g]

Upon Zn plating/stripping, the interfacial resistance increases/decreases by generation/exclusion of voids at the interface. The insertion of carbon/polymer additives/fillers can accommodate volume changes, making homogeneous Zn-ion flux. Thin polymeric/carbon layers are oxidation/reduction-resistant for cathode/anodes. Desolvation (ΔE_{des}) and diffusion (ΔE_{diff}) are the major kinetic barriers that must be considered to prevent Zn corrosion/dissolution processes. CEs/overpotentials (passivation rates, charge-loss, parasitic reactions) are the key parameters for determining the formation of the SEI. It depends on the measuring protocols (current density, time, and temperature), electrolyte compositions, structures, chemistries, and morphologies of gas-diffusion layer/current-collectors (GDL/CC) and Zn-anodes. For example, fluorinated LEs/SEs result in high CEs and smaller overpotentials with forming F-rich SEI. At subzero temperatures, the porous Zn-layer is formed with extensive side reactions, but for high temperatures (≈80 °C), the overpotential and CEs are substantially improved by allowing faster Zn-transport-kinetics with favorable F-rich SEI. $Zn(TFSI)_2$/KOH concentrations considerably improve CEs at 1/6 M concentration. Higher concentrations strongly limit the solubility and ion mobility.[3d] Overpotential increases with current density due to limited ion transport across SEI. Higher current densities generate inhomogeneous voids between the SEI and Zn metal, causing failures with local corrosion and poor CEs. However, F^-/S^--treated Zn(101) anodes and chitosan-cellulosic SEs can overcome this feature by forming stable F-rich SEI.[3] The key to designing the robust interphase for long-term operations at anode/SEs and cathode/SEs is related to the question, "Is it plausible to design SEs that have kinetically beneficial transport properties with lower interface impedance?"

8. Cell Manufacturing

Figure 5 demonstrates the manufacturing of large-scale practical solid-state ZABs. Manufacturing process involves the thin

Table 3. Summary of flexible ZABs for their mechanical and electrochemical properties.

Cell configurations	Cell structures	Electrolyte	Electrolyte stress/strain (MPa/%)	Cathodes/ current collectors	Anodes	OCP [V]	Charge-discharge cycles	Current rate [mA cm^{-2}]	Capacity [mAh g^{-1} @mA cm^{-2})	Mechanical bendings cycles	Bending angle (degree)	Bending time (h)	Discharge voltage (V)	Power density (mW cm^{-2})	Refs.
CPS//CBCs// Zn//CBCs//CPS	Sandwiched pouch cells	CBCs membrane	112/90	CPS/SUS mesh	S,F-based Zn	1.51	6000	25	371@25	6000	0-180	800	1.28	459	[3a]
Mn/Fe-HIB-MOFs//FBN//Zn	Single planar pouch cells	FBN membrane	110/25	Mn/Fe-HIB-MOFs/SUS	Nano-patterned Zn	1.5	3600	10	750@5	2000	0-180	4.16	1.31	193	[9a]
Co_3O_4//nano-SFQ//Zn	Sandwiched cells	Nano-SFQ QSGPEs	–	Co_3O_4/Ni mesh	Zn foil	1.43	450	1	191.3 mAh	25	0-180	50	1.24	104.2	[21]
Co_3O_4//nano-SFQ//Zn	Wire type	Nano-SFQ QSGPEs	–	Co_3O_4/Ni mesh	Zn foil	1.43	90	1	–	20	0-180	50	–	–	[21]
Pt+RuO_2// PANa//Zn	Single planar cells	PANa hydrogel	0.007/400	Pt+RuO_2/Carbon cloth	Zn foil	1.42	800	1.42	795@1	6	0-90	1	1.25	88	[29]
Co_3O_4-NCNT// cellulose//Zn	Single planar cells	Cellulose film	–	Co_3O_4-NCNT/SUS	Zn powder	1.45	1500	25	652.6@5	4	0-120	–	–	160.7	[40]
MPZ-CC@CNT// PVA//Zn	Single planar cells	PVA gel	–	MPZ-CC@CNT/Ni foam	Zn foil	1.47	1800	–	860@25	3	0-120	–	–	160	[41]
GH-BGQD2// PVA//Zn	Single planar cells	PVA gel	–	GH-BGQD2/Ni foam	Zn foil	1.4	300	10	687@10	45	0-180	15	1.2	112	[42]
Co@N-PCP//G-CyBA/PAAm SP-DN//Zn	Wire type	G-CyBA/PAAm SP-DN	0.46/4600	Solid-state secondary	Zn foil	1.35	600	2	800@5	1000	0-180	–	1.30	125	[44]
Nitride/N-Ti_3C_2// PVA//Zn	Fiber type	PVA gel	0.05/20	Nitride/N-Ti_3C_2/ carbon fiber	Zn foil	1.32	9	5	570@5	9	0-180	3	1.2	–	[45]
Co SA@NCF// PVA//Zn	Fiber type	PVA gel	–	Co SA@NCF/- carbon cloth	Zn/carbon cloth	1.41	90	3	530.17@6.25	14	0-180	2.22	1.2	53	[46]
NCNF-1000// PVA//Zn	Single planar cells	PVA gel	–	NCNF-1000/Ni foam	Zn foil	1.256	36	2	378	36	0-180	6	1.0	–	[47]
S-C_2NA// cellulose//Zn	Single planar cells	Cellulose film	–	S-C_2NA/SUS	Zn foil	1.47	230	10	695@5	18	0-180	6	1.12	187	[48a]
$CoS_{1-\delta}/SnS_{2-\delta}$// CBCs//Zn	Single planar cells	CBCs	–	$CoS_{1-\delta}/SnS_{2-\delta}$/SUS	Zn foil	1.51	720	50	810@20	30	0-180	5	1.2	229	[48b]
PEMAC@NDCN// CBCs//Zn	Single planar cells	CBCs	–	PEMAC@NDCN	Zn foil	1.5	2580	25	806@20	48	0-180	8	1.27	211	[48c]
CuSA@HNCNx// FBN//Zn	Single planar cells	FBN membrane	–	CuSA@HNCNx/CC	Zn foil	1.51	1500	25	793@25	1000	0-180	2	1.23	202	[48d]

(*Continued*)

Table 3. (Continued)

Cell configurations	Cell structures	Electrolyte	Electrolyte stress/strain (MPa/%)	Cathodes/ current collectors	Anodes	OCP [V]	Charge-discharge cycles	Current rate [mA cm^{-2}]	Capacity [mAh g^{-1} @mA cm^{-2}]	Mechanical bendings cycles	Bending angle (degree)	Bending time (h)	Discharge voltage (V)	Power density (mW cm^{-2})	Refs.
PS-CNF// PVA//Zn	Single planar cells	PVA gel	–	PS-CNF/CC	Zn foil	1.25	–	2	690@2	100	0-180	2	1.15	–	[48e]
Cu_3P/CoP// PVA//Zn	Single planar cells	PVA gel	–	Cu_3P/CoP/Ni foam	Zn foil	1.35	–	–	765.6	–	0-180	1	1.2	–	[48f]
CoFe/Fe_3C-T_2// PVA-CMC//Zn	Single planar cells	PVA-CMC gel	0.090/140	CoFe/Fe_3C-T_2/GDL	Zn foil	1.43	–	5	–	60	0-90	4	1.1	66	[48g]
CoFe-FeNC// PAA-CNF//Zn	Single planar cells	PAA-CNF gel	–	CoFe-FeNC/Ni foam	Zn foil	1.4	200	0.2	748.8@2	11	0-90	3.5	1.2	53.72	[48h]
$Mg_{0.1}Co_{0.9}$—NC// PVA//Zn	Single planar cells	PAA gel	–	$Mg_{0.1}Co_{0.9}$—NC/Ni foam	Zn foil	1.45	85	5	801@5	15	0-180	2	1.12	148.6	[48i]
J—CeO_2/ZCS// PVA//Zn	Single planar cells	PVA gel	–	J—CeO_2/ZCS/Ni foam	Zn foil	1.40	60	–	–	–	0-135	–	–	117.6	[48j]

film loading of graphene/carbon (G/C) by thermal-vaporization processes, continuous slurry mixing and slurry-casting over the G/C-coated GDL/CCs, roll-to-roll processing of air-cathodes with GDL/CCs, lamination of SEs and air-cathodes (air-cathode + SEs), stacking/winding of electrodes with porous air-permeable-layers, assemble Zn-anode in sandwiched-structures, and cell-packaging.

8.1. Electrodes Processing

Air-cathodes are fabricated by dry-electrode and slurry-casting with roll-pressing processes (Figure 5a). Active-cathodes are mixed by binders, conductive additives (carbon-black), and solvents (N-Methyl-2-pyrrolidone/other-organic), then subsequently slurry-casted on the freestanding G/C-coated GDL with roll-to-roll pressing and drying. For dry electrodes, the homogeneously mixed powders without solvents undergo sequential loading and room-temperature/hot-rolling until the desired thickness. Dry processing allows the dense packing of cathode particles compared to slurry mixtures, illustrating improved charge/mass-transfer-kinetics. Heating rollers mitigate the required applied pressures, facilitating the scalability of dry processing. Two types of Zn-anodes, such as powders or metal foils, can be employed. Powder-based Zn-anodes are fabricated by similar air-cathode slurry-casting processes. Zn-metal foils (50–300 µm) are pretreated for fluorine/sulfur chemical passivation. Sputtered metallic Zn over the carbon cloths is also a favorable approach with preferred thickness. SEs membranes (≥30 µm) are prepared by self-regulating membrane-polymerization or layer-by-layer method with in situ polymerization over the air-cathodes or Zn-anodes and vacuum-drying.

8.2. Cell Stacking

Minimally modified, available commercial types of equipment, such as Z-/sheet-stacking and winding for cylindrical/prismatic and pouch-type cells, are recommended for fabricating scalable solid ZABs prototypes because of flexible polymeric-hybrid SEs (Figure 5b,c). For cylindrical cells, the winding/cylindrical rolling, including Zn-anode sandwiches laminated air-cathode + SEs, and air-permeable layers for both sides of air-cathodes (Figure 5d). The single or bipolar stacked pouch cells are fabricated using Z-stacking with freestanding air-cathode + SEs electrodes sandwiched for Zn-anodes and air-permeable layers (Figure 5e). Although one can choose the cell stacking configuration between asymmetric (Cathode + SE + Zn) and symmetric (Cathode + SE//Zn//SE + Cathode), conventional asymmetric design causes several misalignment concerns that induce cell failures, poor-cell-energy/power metrics, and requires high tolerances for space margin at the cell edges. Mechanical strengths of SEs are critical for Z-stacking tools; thus, the optimal pressure along the axial direction of Z-stacks is required to adjust tensile forces applied to SEs. Z-folding with laminated symmetric configurations can eliminate the direct contact of anodes/cathodes and critically reduces inactive components such as Zn-metal, tabs, and packing materials. This strategy enhances overall packing density and cell-level energies by two to three times. Then, cells need to be moderately

Table 4. Comparison of homemade, coin, and pouch cells for their key parameters and related challenges.

Parameter	Homemade Cells	Coin Cells	Single/Multilayered Pouch Cells	Challenges
Required material quantities	1–10 mg cm^{-2} of cathode over porous CC (carbon paper or cloth, SUS mesh, Ni foams) for cathode testing	1–3 mg cm^{-2} materials required over porous CC for cathode testing	Depends on the electrode coating structure and process: 10–100 g of materials >100 cm^2	Pre-milling of carbon black and catalysts may influence the porosity of electrodes. Scalable fabrication for excellent materials.
Electrode design	One side coating in spherical or square shapes depending on the electrodes (single or double cells, Swagelok)	One side coating in spherical shape as per coin cell dimensions	One side coating over CC	Development of coating and drying processes for uniform thickness without penetration through CCs (thickness, density, mass loading). Avoid penetration through CCs.
Cathode ink fabrication process	Hand grinding in agate mortar with/without excess carbon and binder is often utilized.	Superior grinding and mixing methods such as ball-milling, and swing-mills with applying forces with binder.	Well-pre-mixing, grinding, and blending with binders are critically necessary (> 50 mL)	Homogeneous and robust suspensions of binders, solvents, conductive additives, and active materials for large scale. Shearing forces for >50 mL batch is even more challenging or requires additional supporting equipment for the swing mill.
Cathode coating process	Doctor blade coating or spray coating	Table-shaped coater (20 × 30 cm^2 per sheet)	Comma bar coating or slot die	In comma bar coating, agglomeration of particles occur upon processing period resulting in heterogeneous active materials coatings. Homogeneous gas-free inks are necessary to avoid clogging in slot die.
Potential drop and intrinsic resistance	Intrinsic cathode layer, interface, and electronic contact resistances for total cathode area. It depends on the type of CCs, electrode layers, and tap welding resistances as well.	Intrinsic cathode layer and electronic contact resistances	Total intrinsic resistance depends on the type of CCs, electrode coating layers, and tap welding resistances	Transitions of different materials/CCs (i.e., carbon cloth, SUS mesh, Ni foam) or Zn-anodes in the pouch owing to raised ohmic losses for electrodes. Metal tabs welding over carbon, SUS mesh, or Ni foam CCs and Zn anode is critically difficult.
Required excess electrolytes	>50–200 mL mg^{-1} electrolyte amount with/without flow is utilized for respective cell structures	30–50 µL mg^{-1} electrolyte depends on the separators porosity and vapor pressure of solvents	<3 µL mg^{-1} lower electrolyte loading is required in pouch cells than homemade or coin cells, which significantly reduces the dead volume to obtain higher energy densities	Reduction of the dead volume in homemade and coin cells due to the large size of homemade cells and spacer in coin cells. Pouch cells can significantly minimize the dead volume by using bipolar stacking.
Zn excess	500–2000 µm thick Zn is utilized with N/P of >50, E/A >25 µL mg^{-1}, and E/C >150 µL mg^{-1} (in solid or liquid ZABs)	200–300 µm thick Zn with N/P of >20 (in solid or liquid ZABs)	50–150 µm Zn thickness with N/P of 2–3, E/C <8, and E/A >2.6 is more preferable for solid ZABs	Excess Zn severely decreases the energy density of homemade and coin cells. Electrolyte depletion (water retention properties) and increased cycle numbers with excess electrolytes and Zn. Retention of stable interface for cathode/solid electrolyte/Zn in pouch cells with competitive air penetration.

(*Continued*)

Table 4. (Continued)

Parameter	Homemade Cells	Coin Cells	Single/Multilayered Pouch Cells	Challenges
Electrolyte filling	Immersion of electrodes in the electrolytes	Adding droplets by pipette on single-layered electrodes	Vacuum sealing is required for whole stacks interface or soaking of electrolytes	Obtain uniform electrolyte interface for multilayered cells
Dead volume (volume of cell outside cell stacks)	Highest dead volume >50–200 mL	High dead volume due to spacer	Depending on the stack's design and number of layers, it has the lowest dead volume.	Formation of diffused ZnO, zincate or hydroxides, or other secondary products implies poor. CEs, energy/rate capacities, and degradation of electrolytes or active materials are unable to use
External pressure	External pressure is utilized by fixing the acrylic top/bottom cell parts by external tightening of screws will change severely external pressure or flowing electrolyte case pump flow rates.	No constant pressure for fixed volume without springs. Pressure is well modified with springs by increasing dead volume.	Pouch cells require the application of external pressure in the range of 10–200 psi.	Stabilization of volume changes, porosity, and ion-transports
Role of porosity of cathodes/CC	Air penetration via CC/cathode is critically required to process redox reactions. Cathode swelling and lower oxygen flow can calendar cycling.	Air penetration via CC/cathode is critically required to process redox reactions. Cathode swelling and lower oxygen flow due to spacer in coin cells.	Porosity and swelling characteristics a key parameters during charge-discharge processes	Insertion of additional Air permeable layer in the multilayered structures. Avoid electrical contact of each CC for bipolar stacks. Tab welding for both electrodes.

pressed by uniaxial, areal, or isostatic pressing to improve the interfaces.

The 1–10 Ah-scale, cylindrical (A-to-AAAA types) and pouch-cells (10–120 cm^2 cell areas) were reported using a symmetric design of CuP_xS_y//Chitosan-biocellulose/Zn(101) with 300–500 Wh kg_{cell}^{-1} cell-level energies. 10-Ah pouch cell reveals 1000 cycles lifetime with 89% capacity retention with GDL and pressure of 200 psi.[3a,c] Considering the wide variety of recent impactful lab-scale findings, a few breakthroughs ensure the possibility of transferring toward commercial prospects. Lab-scale research focuses on the materials design and kinetics for small-capacity; however, it lacks practical verification of prototypes relevant for industrial evaluation. An effective balance between academia and industry is highly desirable, so we suggested the key performance metrics for transitions from lab to industrial-scale of realistic ZABs featuring perspective insights of electrode materials (**Tables 5–7**).

9. Future Insights

For commercial cells, the specific and volumetric energies, cycle life, and harsh-temperature operations are the major key parameters for battery developments for EVs, EDs, and eVTOL.

9.1. Materials Scalability

Materials-level scalability for solid ZABs concerns the SEs, cathodes, and Zn-anodes with their specific capacity (C_{SP}) utilization ratios (Tables 5–7). Theoretical energy is calculated from electrochemical reactions with constant stoichiometric anode-to-cathode-materials ratios, whereas practical energy is determined from measured capacity, cell voltages, and total cell mass/volume. Thus, the decisive factors are mass ratios, utilization, and output voltages. Realizing specific cell energy of 100–500 Wh kg^{-1} coupled with patterned Zn-anodes, desired cathode-mass-loading, and electrolyte amount has been reported in Zn-air pouch cells.[9a] To achieve a capacity of 371 mAh g^{-1} (66% of theoretical capacity), CuP_xS_y cathodes with ≥15 mg cm^{-2} (100 µm-thickness) is recommended.

Commercial standards clarify the key parameters, such as the total-capacity pairing of anode-to-cathode ratio (N/P), electrolyte/cathode ratio (E/C), electrolyte/anode ratio (E/A), mass-ratios of binders, carbon-black, GDL/CC, packing-materials. Lab-scale considers an ideal mass-loading (1–2 mg cm^{-2}); however, practical cells require 10–15 times higher mass-loading (10–30 mg cm^{-2}). Low mass-loading mitigates kinetics-barrier with unrealistic high-rate performance, but adopting 5–10 mg cm^{-2} should be the research focus for practical demonstration. Lab-scale ZABs use excess Zn (500–2000 µm-thick) with poor areal capacity (0.5 mAh cm^{-2}) and show very poor Zn-utilization (<1%) with severe misalignment in the cathode capacity. For upscaling ZABs, high-areal-capacity (5–10 mAh cm^{-2}) of cathodes with thin anodes (100–200 µm) is essential to ensure minimal stack layers for obtaining necessary specific energies by decreasing the volume and weight of inactive materials. Ultrathin (10–50 µm) Zn-anodes severely limit the capacities and cycling, similar to Li-metal batteries. The wettability and quantity of SEs will control the ZAB's performance. Thus, the N/P, E/C, E/A, and C_{SP}

Figure 4. Illustration of key structural parameters for design of cathodes, electrolytes, anodes, separators, binders, and cell manufacturing for solid-state ZABs.

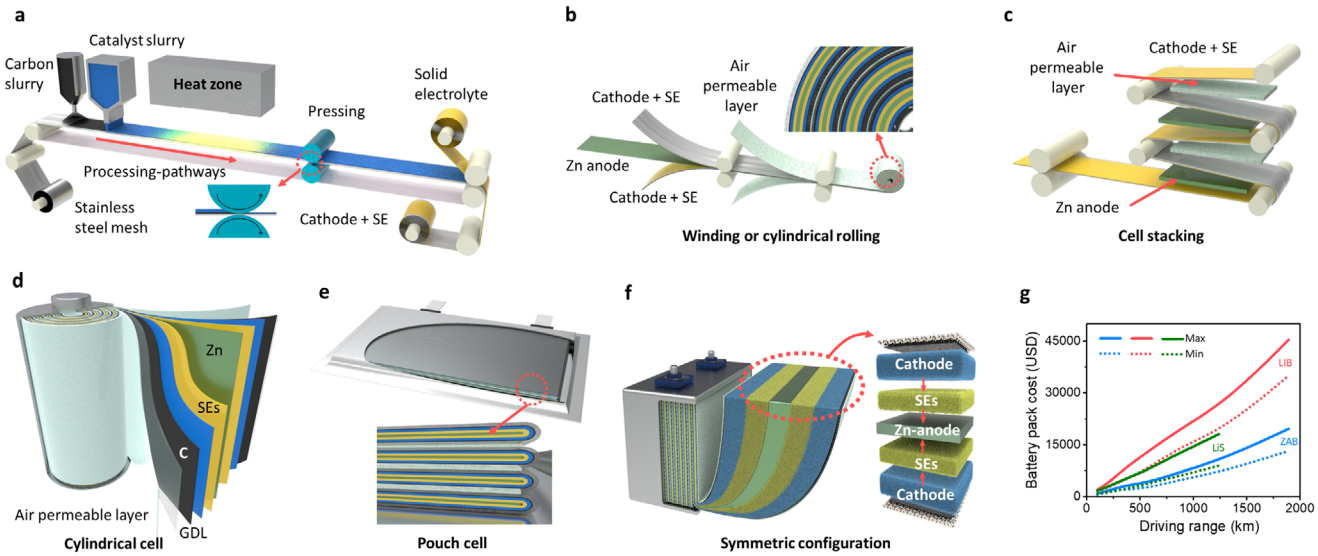

Figure 5. Schematics displaying the cell manufacturing, processing, and cost analysis for solid-state ZABs. a) The fabrication of cathode-electrolyte electrodes includes a continuous slurry coating of the thin carbon layer and cathode materials (including active materials, binder, and carbon black) on the gas-diffusion layer (GDL), calendaring, drying, and densification; then, follows the stacking of solid electrolytes/separators. b) Winding/cylindrical rolling of Zn-anode and cathode-electrolyte electrodes with laminating the air-permeable layers. c) Z-stacking of Zn-anode sandwiched between cathode and solid electrolyte (SE) electrodes in parallel configurations. d) Assembly of ZABs includes winded electrodes and packaging in the cylindrical/prismatic cells. e) Assembly of ZABs includes parallel Z-stacking and packaging in the pouch cells. f) Schematic of cell design under symmetric configurations. g) Projected LIBs, lithium-sulfur (LiS), and ZABs battery pack-level costs with driving range for EVs. Solid and dotted lines denote the probable span of driving range and battery pack cost. Reproduced with permission.[3c] Copyright 2023, Wiley.

Table 5. The state-of-the-art liquid (alkaline, neutral, acid, and hybrid electrolytes) and solid-state reversible Zn-air batteries.

Cathode// Anode	Electrolyte	Battery type	Current density (mA cm^{-2})[a]	Zn mass (g)[d]	Consumed Zn mass [g][a,b]	Cell nominal voltage [V][a]	Active cell area [cm^2]	Reported discharge capacity [mAh g^{-1}][a]	Energy density [Wh kg^{-1}][a,b]	Calculated capacity [mAh g^{-1}][h]	Cathode mass [g][e]	Electrolyte mass [g][f]	Separator mass [g]	Package mass [g][c]	Total mass [g]	Cell-level capacity [mAh g^{-1}][g]	Cell-level energy density [Wh kg^{-1}][g]	DOD/SOC [%]	Charging rate [mA cm^{-2}]	Battery operational life [h/cycles/mA cm^{-2}][d]	Refs.
CPS//Zn	CBCs membrane	Solid-state secondary	25	1	–	1.53	9	371	460	439	0.405	1.146	–	0.459	3.01	371	460	20 & 70	25,50,100,200	800/ 6000/25	[3a]
Mn/Fe-HIB -MOFs//Zn	FBN membrane	Solid-state secondary	5	3.3	1.2	1.44	15	750	975	128.76	0.240	3.45	–	1	7.99	112.64	146.43	5	25	600/ 3600/25	[9a]
FeCo NiSx//Zn	6 M KOH	Alkaline secondary	20	–	–	1.43		3.24 Ah	53.8 cell-level	–	–	–	–	100	–	–	–	<5	10, 100200400	1200/ 2000/10	[9d]
Co_3O_4//Zn	Nano-SFQ QSGPEs	Solid-state secondary	1	0.44	–	1.43	2	191.36 (mAh)	–	–	0.25	2.0	–	1	3.25	58.88	73.6	<5	1	450/ 450/1	[21]
Pt+ RuO_2//Zn	PANa hydrogel	Solid-state secondary	1	1.2	0.61	1.42	5	795	952	150.92	0.0175	2.154	–	1	4.3715	116.39	139.38	5	2	160/ 800/2	[29]
Co_3O_4-NCNT//Zn	Cellulose film	Solid-state secondary	5	1.2	0.8	1.45	6	652.6	847.6	143.2	0.096	1.35	–	1	4.646	112.37	145.95	5	25	500/ 1500/25	[40]
MPZ-CC@CNT//Zn	PVA gel	Solid-state secondary	25	1.2	0.61	1.47	5	860	946	160.26	0.0175	2.154	–	1	4.3715	116.39	139.38	5	50	600/ 1800/50	[41]
GH-BGQD2 //Zn	PVA gel	Solid-state secondary	10	0.4	0.21	1.4	4	687	810	63.61	0.152	1.716	–	1	3.268	44.15	52.06	5	5, 10	300/ 100/10	[42]
α-$Co(OH)_2$-Ru//Zn	6 M KOH	Alkaline secondary	5	2.8	1	1.36	2	973.5	1070.85	80.45	0.125	10	–	100	112.925	3.12	2.1	<5	5	66.66/ 400/5	[43]
Co@N-PCP //Zn	G-CyBA/-PAAm SP-DN	Solid-state secondary	5	4.5	0.25	1.47	12.57	800	960	20.67	0.1760	5	–	1.0	10.676	18.74	22.50	5	2	100/ 600/2	[44]
Nitride/N-Ti_3C_2//Zn	PVA gel	Solid-state secondary	10	0.8	0.14	1.325	7.79	570	627	51.87	0.047	2	–	0.5	3.347	23.84	26.22	< 1	5	3/9/5	[45]
Co SA@NCF//Zn	PVA gel	Solid-state secondary	6.25	0.084	0.032	1.41	3	530.17	646.81	8.154	0.0036	2	0.001	1	3.08	5.51	6.722	< 3	6.25	15/90/6.25	[46]
NCNF-1000//Zn	PVA gel	Solid-state secondary	2	0.22	0.11	1.256	1	378	378	7.92	0.032	5	–	1	6.252	6.66	6.66	< 5	2	6/72/2	[47]
Co/CNWs/ CNFs//Zn	6 M KOH	Alkaline secondary	5	3.3	1.2	1.46	2	823	1020.5	73.83	0.076	10	–	100	113.376	8.71	10.80	5	5	1500/4500/5	[49]
Ir@Co_3O_4//Zn	6 M KOH	Alkaline secondary	20	2.5	1	1.45	7.065	712	801	70.74	0.5	7.065	–	100	110.065	6.47	7.28	1.1	20	210/70/20	[50]
NiFe-PBA//Zn	6 M KOH	Alkaline secondary	10	2.5	0.5	1.4	2	775	891	30.98	0.007	10	0.001	100	112.508	3.44	3.96	< 5	10	2000/10	[51]

(*Continued*)

Table 5. (Continued)

Cathode// Anode	Electrolyte	Battery type	Current density (mA cm^{-2})[a]	Zn mass (g)[d]	Consumed Zn mass [g][a,b]	Cell nominal voltage [V][a]	Active cell area [cm^2]	Reported discharge capacity [mAh g^{-1}][a]	Energy density [Wh kg^{-1}][a,b]	Calculated capacity [mAh g^{-1}][h]	Cathode mass [g][e]	Electrolyte mass [g][f]	Separator mass [g]	Package mass [g][c]	Total mass [g]	Cell-level capacity [mAh g^{-1}][g]	Cell-level energy density [Wh kg^{-1}][g]	DOD/SOC [%]	Charging rate [mA cm^{-2}]	Battery operational life [h/cycles/mA cm^{-2}][d]	Refs.
Fe_1/ d-CN//Zn	6 M KOH	Alkaline secondary	10	9.6	0.45	1.5	1	770	890	17.57	0.121	10	–	100	119.721	2.894	3.35	< 3	1	20/60/1	[52]
Co_2P/ CoN//Zn	6 M KOH	Alkaline secondary	20	1	0.4125	1.36	1	649.6	844.5	44.61	0.006	5	–	100	106.006	2.528	3.29	< 5	5	47/95/5	[53]
Asy-NiFe//Zn	6 M KOH	Alkaline secondary	25	4	0.4	1.66	2	806	685.1	33.57	0.6042	5	–	100	109.6042	2.941	2.5	< 5	10	3400/566/10	[54]
CoDNG900//Zn	6 M KOH	Alkaline secondary	10	8	0.25	1.45	2	669	785	12.77	0.102	5	–	100	113.102	1.48	1.74	< 5	10	667/2000/10	[55]
FeCo SAs/ N-C//Zn	6 M KOH/ 3 M H_3PO_4	Hybrid secondary	0.1	1	0.159	2.1	1	686	1345	21.51	0.007	4	0.002	150	155.072	0.7034	1.386	< 5	1	110/330/1	[56]
Co_9S_8 @N,S-C//Zn	6 M KOH	Alkaline secondary	20	1.1	0.25	1.51	0.785	862	991	19.37	0.0262	10	–	100	111.1262	1.94	2.23	< 5	10	110/660/10	[57]
*Super P//Zn	$Zn(TFSI)_2$ -LiTFSI	Aqueous secondary	50 mA g^{-1}	–	–	1.25	1	1000	1250	–	0.001	–	–	3	3.02	0.3311	0.4966	–	50	200/50 mAg^{-1}	[58]

[a] defines the stated values from previous reports; [b] defines the calculated values from the reported electrochemical performances (if it is not mentioned in the respective articles); [c] denotes the cell pack mass derived from commercial Acrylic/Teflon-based structures; [d] defines the determined Zn anode mass by using the standard thickness of Zn foil (0.3 and 0.5 mm; 0.22 and 0.4 g cm^{-2}); [e] Evaluated cathode mass from the stated mass loadings for the different CCs such as carbon paper or cloth and SUS mesh [f] Liquid cells with excess electrolytes from 1 to 10 mL with several times electrolyte exchange; [g] Determined cell-level capacities and energy densities.[3a,c]; [h] Evaluated cell capacity without consideration of packing materials mass.

Table 6. The transformation from lab-scale to commercial-level practical ZABs.

Parameters	Laboratory scale	Pilot prototypes	Commercial large scale
Cell capacity	1 mAh–1 Ah	100 mAh–10 Ah	>10 Ah cells for kWh packs
Fabrication methods	Manual in ambient conditions	Semi-automated in ambient environments	Fully automated in ambient environments
Research insights	Materials rational design and compatibility analysis	Chemistry and design confirmation	Cost reduction and quantity optimization
Critical issues	Inappropriate analysis, access to resources	Scalability and resource supply chains	Emanation of defects with quality control

are crucial in scaling up ZABs. Volumetric energy is another prerequisite for scaling up ZABs; thus, developing high-areal-capacity, tap-density electrodes needs to be explored by optimal processing of high-mass-cathodes, ultrathin-SEs, and surface structures/particle distributions. Binder content, yield stress, and GDL/CC-wettability critically decide the ion/electron conduction of practical-scale cathodes. A manufacturing process with reliable homogeneity, compatibility, mechanical strength, and energy density is critical to scaling cathodes for solid-ZABs. For the commercial viability of ZABs, the electrochemical performances must be evaluated with realistic capacities >1 Ah to match the commercial prototypes and progressively scale up for 5–20 Ah capacities.

Regarding the scalability of SEs, the polymeric host frameworks, cross-linked functional groups, structural phases, nano/micro-structures, and ion-transport pathways affect the ion-conductivity and charge/mass-transfer kinetics. Nanostructured SEs enable large surface areas with numerous ion transport channels, high rate capabilities, improved capacity utilization with limited swelling, and increased water retention

Table 7. The key parameters from material level to practical scale.

Electrodes/strategies		Key performance metrics							Commercial energy storage technologies								
		Materials utilization	Corrosion reactions inhibition	Ion transport	Catalytic activities	EWs	Uniform Zn deposition	Electrical conductivity	Operating voltage	Areal capacity	Coulombic efficiency	Power density	Energy density	Energy efficiency	Voltage efficiency	Cycle lifetime	Cost
Anode	Artificial SEI	■	■	■	■	■	■	■	■	■	■	■	■	■	■	■	■
	Design structures	■	■	■	■	■	■	■	■	■	■	■	■	■	■	■	■
Cathode	Intrinsic	■	■	■	■	■	■	■	■	■	■	■	■	■	■	■	■
	Defects control	■	■	■	■	■	■	■	■	■	■	■	■	■	■	■	■
	Size control	■	■	■	■	■	■	■	■	■	■	■	■	■	■	■	■
	Composites	■	■	■	■	■	■	■	■	■	■	■	■	■	■	■	■
Electrolyte	High concentrated	■	■	■	■	■	■	■	■	■	■	■	■	■	■	■	■
	Additives based	■	■	■	■	■	■	■	■	■	■	■	■	■	■	■	■
	Solid-state	■	■	■	■	■	■	■	■	■	■	■	■	■	■	■	■
	Liquid	■	■	■	■	■	■	■	■	■	■	■	■	■	■	■	■
Cell configuration	Membrane-free	■	■	■	■	■	■	■	■	■	■	■	■	■	■	■	■
	Planar	■	■	■	■	■	■	■	■	■	■	■	■	■	■	■	■
	Asymmetric	■	■	■	■	■	■	■	■	■	■	■	■	■	■	■	■
	Symmetric	■	■	■	■	■	■	■	■	■	■	■	■	■	■	■	■

■ Significantly improved; ■ Improved; ■ No relevance; ■ Partial degradation; ■ Severe degradation.

compared to micro/macro-structured SEs using facile polymerization reactions. Micro/macro-structured SEs undergo severe hydration and hydrolysis reactions with CO_2, NH_3, HCl, or H_2S gases and excess swelling, facilitating poor interface compatibility and energy/power characteristics.

Chitosan- and cellulose materials were suggested as one possible candidate for large-scale production of SEs due to their intrinsic properties such as water-binding strengths/wettability, permeability, scalable nanostructures, chemical/physical-stability, cost-effective, interfacial-reaction compatibility, thermodynamic-properties, and environmental-safety/biodegradation after cell-operations. Hybrid SEs based on chitosan/cellulose with optimal concentrations/stoichiometry and water-organic solvents offer practical pathways for ZABs with continuous ion flux. For dendrite-free Zn-anode operations, Sand's ideal condition and theoretical demonstrations require the SEs to satisfy the condition, "the shear modulus of SEs should be greater than that of a Zn-anode ($G_{SEs} > G_{Zn}$) and the lower surface diffusion barriers with high surface energies".[3a,c] Lab-scale reports mostly utilize excess SEs of 500–5000 µm thickness that can readily regulate the density, internal defects, and battery assembly; however, the specific-capacity/energy is evaluated based on the consumed mass of Zn, which is critically far-away from industrial requirements. Excess SEs severely degrade (10–100 times) the specific energies of the full cells required for commercial-scale applications. Realizing industrial-standard SEs (ultrathin of 30–100 µm) with batch production is the most critical challenge with superion-conductivity, mechanical strengths, and interfacial homogeneity to fulfill high-energy batteries.

9.2. Fast-Charging

Electrochemical operations of ZABs include oxygen (O_2)-diffusion, dissolution/emission of O_2, electrochemical oxidation/reduction of O_2, intermediates, and discharge products for the electrodes and SEs. Among these, finding the critical resistance-contributing steps is the key requirement to achieve high rate-capability and fast charging. Effective GDL is necessary for practical current densities since the O_2 diffusion is a rate-limiting step for air cathodes. Failure of catalysts realizes fast-charging of ZABs, generating voluminous O_2 bubbles and hindering the interactions among the catalysts and reactants with instigating catalysts dropping off the gathered electrodes.[9b] Deficient active sites and poor inherent OER activities of the catalysts are the major obstacles that cause difficulty in delivering poor overpotentials for higher current densities. Powder-based catalysts are challenged by the clumsy process steps over CCs, which require conductive carbon and additional polymeric binders. Then, it inevitably suffers from increased resistance, shielded active sites, poor mass/charge transport kinetics, and conductive carbon oxidation. Carbon oxidation results in severe degradation of ZABs performances with limiting cycle lifespan.[9c] Further, it undergoes worse with ZABs charging for higher current densities. Utilizing carbon-free catalysts is a realistic strategy to avoid the irretrievable oxidation of carbon, delaying the cycle lifespan.[9d] Employing self-supported electrodes with superior metallic catalysts (oxides, sulfides, nitrides, sulfates, etc.) with minimal carbon (<3%) declines the catalysts shedding, deficient mass loadings, unrecoverable carbon corrosion for the realization of fast-charging ZABs over a longer lifespan. For example, metal sulfides have superior OER activities by self-reconstruction for metal (oxy)hydroxide real active sites. Surface atomic configurations and exposed crystal planes of reconstructed metal (oxy)hydroxides modulate the element compositions and structures with a tailoring coordination environment, and electronic structures realize higher OER performance. Multimetallic (oxy)hydroxides have also been identified to perform superior OER activities to those of single counterparts. Multimetallic (FeCoNiSx) (oxy)hydroxides have unique structures generated by surface reformation of amorphous multi-metallic sulfides with abundant dangling chemical bonds and structural defects. Thus, it extends high current densities (10, 100, 200, and 400 mA cm^{-2}) for lower OER overpotentials aiming for fast charging for 2000, 150, 280, and 175 cycles.[9e] Table 5 summarizes the charging current densities with cycle lifespan and validates that ZABs can operate at 25, 50, 100, and 200 mA cm^{-2} charging current density for 6000, 4500, 1500, and 1000 cycles for CPS-based catalysts. Mesoporous hybrid catalysts obtained fast charging by 50 mA cm^{-2}; however, it is limited to 1800 cycles.

Mitigating interfacial instabilities, mass/charge-transfer resistance, polarization gradients, and depletion of electrolytes realize the high current-density operations. Molecular structures, functional groups, and solvent/salts of SEs, conformal interfaces of Zn/SEs and cathode/SEs determine the critical current density (CCD) considering parasitic Zn-dendrites and rising rate-capability (one to five orders in magnitude). Increasing CCD beyond the O_2-diffusion (rate-limiting) step with high capacity retention and safety is desirable for fast-charging viability.

9.3. Cell-Energy Metrics

Based on our work, we suggest the key battery parameters required for high-energy practical ZABs (**Table 8**): 1. For 100 Wh kg^{-1} cell-level energy density, the cathode mass-loading ≥ 3 mg cm^{-2}, E/C ≤37, N/P ≤7.5, E/A ≥1.2, and capacity ≥ 0.5 sAh; 2. For 300 Wh kg^{-1}, the cathode mass ≥ 10 mg cm^{-2}, E/C ≤12, N/P ≤2.4, E/A ≥1.4, and capacity ≥ 0.8 Ah; 3. For 500 Wh kg^{-1}, the cathode mass ≥ 15 mg cm^{-2}, E/C ≤8.0, N/P ≤1.8, E/A ≥2.6, and capacity ≥ 1.0 Ah.

9.4. Cost

Figure 5g displays energy and pack-cost characteristics considering materials supply chain/yields, processing, packaging, and other overhead charges. Maximum specific energy of ≥500 Wh $kg^{-1}{}_{cell}$ with a nominal cost of 48 US$ kWh^{-1} for ZABs attracts the emerging EVs market. ZABs project the two to three-times lower-cost (4000–20000 US$ per battery pack) and longest-range EVs (≈2000 km) relative to those of LiS and LIBs (20000-45000 US$). Power, calendar life, and self-discharge rates must also be considered for reliable EVs. Thus ZABs are attractive candidates to replace LIBs in EVs because of decreased range anxiety for relatively reasonable costs. Materials supply chains must be robust for manufacturing because geopolitical instabilities severely disrupt the availability and costs. There are inevitable

Table 8. Principal testing parameters required for lab-scale Zn battery measurements and specifications required for achieving each cell-level energy density.

Parameters/Cell energy [Wh kg^{-1}_{cell}]	Specifications required for each parameter (or each cell-level energy density)
Cathodes	Mass loading with all components (10–20 mg cm^{-2}), GDL/CC thickness
Electrolytes	Electrolyte types, E/C ratios, amount, and thickness for SEs
Separators	Thickness and materials type
Anodes	Mass loading, thickness, N/P ratio (2–3)
Cell dimensions	Cell design types, size, packing, and tab materials
Electrochemical parameters	Operating temperature, power density, specific energy density (>300 Wh kg^{-1}_{cell}), cycling for 40%–80% DOD (>1000 cycles), rate-capacity (20–50 mA cm^{-2}), Coulombic efficiencies (CE) of ≥99.9%
100 Wh kg^{-1}_{cell}	N/P ≤ 7.5, E/C ≤ 37, E/A ≥ 1.2, Cell capacity ≥ 0.5 Ah, Cathode mass ≥ 3 mg cm^{-2}
300 Wh kg^{-1}_{cell}	N/P ≤ 2.4, E/C ≤ 12, E/A ≥ 1.4, Cell capacity ≥ 0.8 Ah, Cathode mass ≥ 10 mg cm^{-2}
500 Wh kg^{-1}_{cell}	N/P ≤ 1.8, E/C ≤ 8.0, E/A ≥ 2.6, Cell capacity ≥ 1.0 Ah, Cathode mass ≥ 15 mg cm^{-2}

pros/cons in commodity prices; however, deep forecasts over future costs of ZABs manufacturing are necessary for sustainable fabrications. Further, battery-waste disposal, solvents, and toxicity are also important parameters to consider. AEMs are ultimately valuable SEs due to water-based processability. Upscaling SE fabrication processes is critical, and solution processing is the best approach. Non-recycled LIBs pose a risk to local environments owing to leakage of eco-toxic components and depletion of limited resources. By contrast, recycling ZABs is economically viable while retaining high efficiency because of non-toxic ingredients and SEs using well-known processes for spent alkaline/Zn-C batteries. However, an in-depth understanding of the principles of green materials design is necessary due to unknown performance degradation, target costs, and separation of cathode/SEs components.

9.5. Testing Standards

ZAB research suffers from arbitrary testing parameters due to a lack of testing standards, inducing the misinterpretation of performances. Numerous ZABs report 5000–10000 cycles-stability; however, poor charge-discharge rates and <5% DOD made it challenging to provide valuable insights for practical ZABs (Table 5). ZABs future research must focus on the performance capabilities of relevant technology standards. We recommend a set of testing parameters such as 1) Cycle life should be measured for 100% DOD at 1C, similar to LIBs standards; 2) Specific-capacity of >1 Ah-scale and areal-capacity (>5 mAh cm^{-2}); 3) Energy density for full-cell weight/volume; 4) High mass-loading of 10–15 mg cm^{-2}; and 5. N/P and E/C ratios are denoted in Table 8. These metrics are not prescriptive and can vary depending on the applications. These standards will accelerate the ZABs toward realistic assessments.

10. Methods

10.1. Calculations of Power Demands for EVs

Velocity profiles are calculated using the vehicle dynamics model for Urban Urban Dynamometer Driving Schedule (UDDS) driving cycles to evaluate the battery power demands. The power of wheels is assessed as:

$$P_{wheels}(t) = \left(m_{EV}\frac{dv(t)}{dt} + m_{EV}g\cos\theta\frac{C_r}{1000}\left(c_1 v(t) + c_2\right) + 0.5\rho_{Air}A_f C_D v^2(t) + m_{EV}g\sin\theta \right) v(t) \quad (1)$$

where, m_{EV} is vehicle mass of 2230 kg, $v(t)$ the velocity in m s^{-1}, θ ~0 the climbing angle, $C_r = 1.75$, $c_1 = 0.0328$, $c_2 = 4.575$, ρ_{Air} the air density of 1.225 kg m^{-3}, $A_f = 2.67$ m^2 the front area of vehicle, $C_D = 0.23$ the aerodynamic drag coefficient.

The battery pack power for regeneration braking and traction modes are evaluated as:

Regenerative breaking mode

$$P_{bat} = P_{wheels} \times \eta_{rb} \quad (2)$$

Traction mode

$$P_{bat} = \frac{P_{wheels}}{\eta_T \eta_{md}} \quad (3)$$

where $\eta_T = 92\%$ the transmission efficiency, $\eta_{md} = 91\%$ the electric motor efficiency, $\eta_{rb} = 82\%$ the regenerative breaking efficiency. The estimated pack powers are normalized with total pack energy of 85 and 200 kWh.

Supporting Information

Supporting Information is available from the Wiley Online Library or from the author.

Acknowledgements

This work was supported by the Basic Science Research Program (NRF-2023R1A2C3003788) through the National Research Foundation of Korea (NRF), funded by the Ministry of Science and ICT.

Conflict of Interest

The authors declare no conflict of interest.

Keywords

all-solid-state batteries, cell manufacturing, zinc-air batteries, zinc anode

Received: November 13, 2024
Revised: December 29, 2024
Published online: January 21, 2025

[1] a) https://www.mckinsey.com/industries/automotive-and-assembly/our-insights/battery-2030-resilient-sustainable-and-circular, (accessed: January 2023); b) S. Shinde, N. Wagh, S. Kim, J. Lee, *Adv. Sci.* **2023**, *10*, 2304235; c) N. Wagh, S. Shinde, C. Lee, J. Jung, D. Kim, S. Kim, C. Lin, S. Lee, J. Lee, *Appl. Catal. B.* **2020**, *268*, 118746.

[2] a) https://www.vantagemarketresearch.com/industry-report/metalair-battery-market-1135, (accessed: January 2022). b) https://www.maximizemarketresearch.com/market-report/metal-air-battery-market/189413, (accessed: January 2024).

[3] a) S. Shinde, J. Jung, N. Wagh, C. Lee, S. Kim, D. Kim, S. Lee, J. Lee, *Nat. Energy* **2021**, *6*, 592; b) Q. Wang, S. Kaushik, X. Xiao, Q. Xu, *Chem. Soc. Rev.* **2023**, *52*, 6139; c) S. Shinde, N. Wagh, C. Lee, D. Kim, S. Kim, H. Um, S. Lee, J. Lee, *Adv. Mater.* **2023**, *35*, 2303509; d) A. Grimaud, O. Morales, B. Han, W. Hong, Y. Lee, L. Giordano, K. Stoerzinger, M. Koper, Y. Horn, *Nat. Chem.* **2017**, *9*, 457; e) S. Shinde, C. Lee, A. Sami, D. Kim, S. Lee, J. Lee, *ACS Nano 11*, 347. f) N. Wagh, S. Shinde, J. Lee, *Chem. Commun.* **2024**, *60*, 15015.

[4] X. Yang, T. Liu, S. Ge, E. Rountree, C. Wang, *Joule* **2021**, *5*, 1644.

[5] M. Xu, H. Dou, Z. Zhang, Y. Zheng, B. Ren, Q. Ma, G. Wen, D. Luo, A. Yu, L. Zhang, X. Wang, Z. Chen, *Angew. Chem., Int. Ed.* **2022**, *61*, 202117703.

[6] K. Girma, V. Lorenz, S. Blaurock, F. Edelmann, *Coord. Chem. Rev.* **2005**, *249*, 1283.

[7] a) J. Liu, Z. Bao, Y. Cui, E. Dufek, J. Goodenough, P. Khalifah, Q. Li, B. Liaw, P. Liu, A. Manthiram, Y. Meng, V. Subramanian, M. Toney, V. Viswanathan, M. Whittingham, J. Xiao, W. Xu, J. Yang, X. Yang, J. Zhang, *Nat. Energy* **2019**, *4*, 180; b) S. Randau, D. Weber, O. Kötz, R. Koerver, P. Braun, A. Weber, E. Tiffée, T. Adermann, J. Kulisch, W. Zeier, F. Richter, J. Janek, *Nat. Energy* **2020**, *5*, 259; c) Y. Liu, Y. Zhu, Y. Cui, *Nat. Energy* **2019**, *4*, 540; d) P. Albertus, S. Babinec, S. Litzelman, A. Newman, *Nat. Energy* **2018**, *3*, 16; e) Z. Wang, J. Huang, Z. Guo, X. Dong, Y. Liu, Y. Wang, Y. Xia, *Joule* **2019**, *3*, 1289; f) J. Zheng, Q. Zhao, T. Tang, J. Yin, C. Quilty, G. Renderos, X. Liu, Y. Deng, L. Wang, D. Bock, C. Jaye, D. Zhang, E. Takeuchi, K. Takeuchi, A. Marschilok, L. Archer, *Science* **2019**, *366*, 645; g) L. Cao, D. Li, T. Pollard, T. Deng, B. Zhang, C. Yang, L. Chen, J. Vatamanu, E. Hu, M. Hourwitz, L. Ma, M. Ding, Q. Li, S. Hou, K. Gaskell, J. Fourkas, X. Yang, K. Xu, O. Borodin, C. Wang, *Nat. Nanotechnol.* **2021**, *16*, 902.

[8] a) M. Zhou, S. Guo, J. Li, X. Luo, Z. Liu, T. Zhang, X. Cao, M. Long, B. Lu, A. Pan, G. Fang, J. Zhou, S. Liang, *Adv. Mater.* **2021**, *33*, 2100187; b) D. Yuan, J. Zhao, H. Ren, Y. Chen, R. Chua, E. Jie, Y. Cai, E. Edison, W. Manalastas, M. Wong, M. Srinivasan, *Angew. Chem., Int. Ed.* **2021**, *60*, 7213.

[9] a) S. Shinde, C. Lee, J. Jung, N. Wagh, S. Kim, D. Kim, C. Lin, S. Lee, J. Lee, *Energy Environ. Sci.* **2019**, *12*, 727; b) Y. Kim, A. Lim, J. Kim, D. Lim, K. Chae, E. Cho, H. Han, K. Jeon, M. Kim, G. Lee, G. Lee, H. Ahn, H. Park, H. Kim, J. Kim, Y. Jung, *Nat. Commun.* **2020**, *11*, 4921; c) S. Sultan, J. Tiwari, J. Jang, A. Harzandi, F. Salehnia, S. Yoo, K. Kim, *Adv. Energy Mater.* **2018**, *8*, 1801002; d) F. Pan, Z. Li, Z. Yang, Q. Ma, M. Wang, H. Wang, M. Olszta, G. Wang, Z. Feng, Y. Du, Y. Yang, *Adv. Energy Mater.* **2020**, *11*, 2002204; e) A. Wang, X. Zhang, S. Gao, C. Zhao, S. Kuang, S. Lu, J. Niu, G. Wang, W. Li, D. Chen, H. Zhang, X. Zhou, S. Zhang, B. Zhang, W. Wang, *Adv. Mater.* **2022**, *34*, 2204247.

[10] J. Fu, J. Zhang, X. Song, H. Zarrin, X. Tian, J. Qiao, L. Rasen, K. Li, Z. Chen, *Energy Environ. Sci.* **2016**, *9*, 663.

[11] Z. Xia, S. Yuan, G. Jiang, X. Guo, J. Fang, L. Liu, J. Qiao, J. Yin, *J. Membrane Sci.* **2012**, *390–391*, 152.

[12] J. Zhang, J. Fu, X. Song, G. Jiang, H. Zarrin, P. Xu, K. Li, A. Yu, Z. Chen, *Adv. Energy Mater.* **2016**, *6*, 1600476.

[13] J. Qiao, J. Zhang, J. Zhang, *J. Power Sources* **2013**, *237*, 1.

[14] N. Li, T. Yan, Z. Li, T. Thurn-Albrecht, W. Binder, *Energy Environ. Sci.* **2012**, *5*, 7888.

[15] J. Ran, L. Wu, J. Vorcoe, A. Ong, S. Poynton, T. Xu, *J. Membrane Sci.* **2012**, *415–416*, 242.

[16] J. Wang, Y. Zhao, B. Setzler, S. Carbonell, C. Yehuda, A. Amel, M. Page, L. Wang, K. Hu, L. Shi, S. Gottesfeld, B. Xu, Y. Yan, *Nat. Energy* **2019**, *4*, 392.

[17] Y. Kim, L. Moh, T. Swager, *ACS Appl. Mater. Interfaces* **2017**, *49*, 42409.

[18] J. Chen, *Polymer* **2018**, *141*, 143.

[19] C. Jin, X. Zhu, S. Zhang, *Solid State Ionics* **2019**, *335*, 121.

[20] K. Lewandowski, Malinska, *Solid State Ionics* **2000**, *133*, 265.

[21] X. Fan, H. Wang, X. Liu, J. Liu, N. Zhao, C. Zhong, W. Hu, J. Lu, *Adv. Mater.* **2023**, *35*, 2209290.

[22] M. Xu, H. Dou, Z. Zhang, Y. Zheng, B. Ren, Q. Ma, G. Wen, D. Luo, A. Yu, L. Zhang, X. Wang, Z. Chen, *Angew. Chem.* **2022**, *134*, e202117.

[23] Z. Cao, H. Hu, M. Wu, K. Tang, T. Jiang, *J. Mater. Chem. A* **2019**, *7*, 17581.

[24] M. Tan, B. Li, P. Chee, X. Ge, Z. Liu, Y. Zong, X. Loh, *J. Power Sources* **2018**, *400*, 566.

[25] Y. Zhang, H. Qin, M. Alfred, H. Ke, Y. Cai, Q. Wang, F. Huang, B. Liu, P. Lv, Q. Wei, *Energy Storage Mater.* **2021**, *42*, 88.

[26] L. Ma, S. Chen, D. Wang, Q. Yang, F. Mo, G. Liang, N. Li, H. Zhang, J. Zapien, C. Zhi, *Adv. Energy Mater.* **2019**, *9*, 1803046.

[27] Y. Zhou, J. Pan, X. Ou, Q. Liu, Y. Hu, W. Li, R. Wu, J. Wen, F. Yan, *Adv. Energy Mater.* **2021**, *11*, 2102047.

[28] Z. Pei, Z. Yuan, C. Wang, S. Zhao, J. Fei, L. Wei, J. Chen, C. Wang, R. Qi, Z. Liu, Y. Chen, *Angew. Chem., Int. Ed.* **2020**, *59*, 4793.

[29] Y. Huang, Z. Li, Z. Pei, Z. Liu, H. Li, M. Zhu, J. Fan, Q. Dai, M. Zhang, L. Dai, C. Zhi, *Adv. Energy Mater.* **2018**, *8*, 1802288.

[30] F. Allebrod, P. Mollerup, C. Chatzichristodoulou, M. Mogensen, *Int. Conf. on Hydrogen Production*, Thessaloniki, Greece, June **2011**, p. 181ELE.

[31] H. Bianchi, H. Corti, R. Prini, *J. Solution Chem.* **1994**, *23*, 1203.

[32] H. Dong, J. Li, J. Guo, F. Lai, F. Zhao, Y. Jiao, D. Brett, T. Liu, G. He, P. Parkin, *Adv. Mater.* **2021**, *33*, 2007548.

[33] a) X. Wang, J. Meng, X. Lin, Y. Yang, S. Zhou, Y. Wang, A. Pan, *Adv. Funct. Mater.* **2021**, *31*, 2106114; b) Z. Liu, Z. Guo, L. Fan, C. Zhao, A. Chen, M. Wang, M. Li, X. Lu, J. Zhang, Y. Zhang, N. Zhang, *Adv. Mater.* **2024**, *36*, 2305988; c) X. Zhang, J. Li, Y. Liu, B. Lu, S. Liang, J. Zhou, *Nat. Commun.* **2024**, *15*, 2735; d) D. Zhang, Z. Song, L. Miao, Y. Lv, H. Duan, M. Li, L. Gan, M. Liu, *Angew. Chem., Int. Ed.* **2024**, 202414116; e) M. Yan, X. Zhao, D. Chen, W. Li, L. Liu, Y. Sun, S. Jiao, H. Pan, *Adv. Energy Mater.* **2024**, 2403860.

[34] a) Y. Zhang, J. Howe, S. Yoseph, Y. Wu, N. Liu, *ACS Energy Lett.* **2021**, *6*, 404; b) S. Wang, Q. Ran, R. Yao, H. Shi, Z. Wen, M. Zhao, X. Lang, Q. Jiang, *Nat. Commun.* **2020**, *11*, 1634; c) L. Wang, S. Zhou, K. Yang, W. Huang, S. Ogata, L. Gao, X. Pu, *Adv. Sci.* **2024**, *11*, 2307667; d) C. Liu, Z. Luo, W. Deng, W. Wei, L. Chen, A. Pan, J. Ma, C. Wang, L. Zhu, L. Xie, X. Cao, J. Hu, G. Zou, H. Hou, X. Ji, *ACS Energy Lett.* **2021**, *6*, 675; e) H. Tian, Z. Li, G. Feng, Z. Yang, Y. Yang, *Nat. Commun.* **2021**, *12*, 237.

[35] a) R. Zhao, J. Yang, X. Han, Y. Wang, Q. Ni, Z. Hu, C. Wu, Y. Bai, *Adv. Energy Mater.* **2023**, 2203542; b) M. Cui, B. Yan, F. Mo, X. Wang, Y. Huang, J. Fan, C. Zhi, H. Li, *Chem. Eng. J.* **2022**, *434*, 134688; c) W.

Zhang, Q. Qi, K. Yang, Y. Hu, F. Jiang, W. Liu, L. Du, Z. Yan, J. Sun, *Energy Storage Mater.* **2024**, *71*, 103616.

[36] a) L. Kang, K. Yue, C. Ma, H. Yuan, J. Luo, Y. Wang, Y. Liu, J. Nai, X. Tao, *Nano Lett.* **2024**, *24*, 4150; b) J. Wang, J. Peng, W. Huang, H. Liang, Y. Hao, J. Li, H. Chu, H. Wei, Y. Zhang, J. Liu, *Adv. Funct. Mater.* **2024**, *34*, 2316083; c) D. Lv, Q. Li, P. Wu, X. Zhang, L. Wang, B. Li, N. Gao, Z. Liu, L. Wang, *Langmuir* **2024**, *40*, 11287; d) N. Zhang, S. Huang, Z. Yuan, J. Zhu, Z. Zhao, Z. Niu, *Angew. Chem., Int. Ed.* **2021**, *60*, 2861; e) L. Dong, W. Yang, W. Yang, H. Tian, Y. Huang, X. Wang, C. Xu, C. Wang, F. Kang, G. Wang, *Chem. Eng. J.* **2020**, *384*, 123355.

[37] a) Z. Zhao, J. Zhao, Z. Hu, J. Li, J. Li, Y. Zhang, C. Wang, G. Cui, *Energy Environ. Sci.* **2019**, *12*, 1938; b) S. Wang, Z. Yang, B. Chen, H. Zhou, S. Wan, L. Hu, M. Qiu, L. Qie, Y. Yu, *Energy Storage Mater.* **2022**, *47*, 491; c) H. Peng, C. Liu, N. Wang, C. Wang, D. Wang, Y. Li, B. Chen, J. Yang, Y. Qian, *Energy Environ. Sci.* **2022**, *15*, 1682; d) X. Cai, W. Tian, Z. Zhang, Y. Sun, L. Yang, H. Mu, C. Lian, H. Qiu, *Adv. Mater.* **2024**, *36*, 2307727; e) M. Chen, X. Guo, X. Jiang, B. Farhadi, X. Guo, Y. Zhu, H. Zhang, S. Liu, *Angew. Chem., Int. Ed.* **2024**, *63*, 202410011; f) G. Zhu, H. Zhang, J. Lu, Y. Hou, P. Liu, S. Dong, H. Pang, Y. Zhang, *Adv. Funct. Mater.* **2024**, *34*, 2305550; g) R. Chen, W. Zhang, C. Guan, Y. Zhou, I. Gilmore, H. Tang, Z. Zhang, H. Dong, Y. Dai, Z. Du, X. Gao, W. Zong, Y. Xu, P. Jiang, J. Liu, F. Zhao, J. Li, X. Wang, G. He, *Angew. Chem.* **2024**, *136*, 202401987.

[38] a) P. Xiao, H. Li, J. Fu, C. Zeng, Y. Zhao, T. Zhai, H. Li, *Energy Environ. Sci.* **2022**, *15*, 1638; b) Q. Zhang, J. Luan, X. Huang, Q. Wang, D. Sun, Y. Tang, X. Ji, H. Wang, *Nat. Commun.* **2020**, *11*, 3961; c) X. Yang, C. Li, Z. Sun, S. Yang, Z. Shi, R. Huang, B. Liu, S. Li, Y. Wu, M. Wang, Y. Su, S. Dou, J. Sun, *Adv. Mater.* **2021**, *33*, 2105951; d) X. Guo, Q. Peng, K. Shin, Y. Zheng, S. Tunmee, C. Zou, X. Zhou, Y. Tang, *Adv. Energy Mater.* **2024**, *14*, 2402015.

[39] a) W. Guo, Z. Cong, Z. Guo, C. Chang, X. Liang, Y. Liu, W. Hu, X. Pu, *Energy Storage Mater.* **2020**, *30*, 104; b) J. Chen, X. Qiao, X. han, J. Zhang, H. Wu, Q. He, Z. Chen, L. Shi, Y. Wang, Y. Xie, Y. Ma, J. Zhao, *Nano Energy* **2022**, *103*, 107814; c) Y. An, Y. Tian, S. Xiong, J. Feng, Y. Qian, *ACS Nano* **2021**, *15*, 11828; d) X. Chen, Z. Zhai, T. Yu, X. Liang, R. Huang, F. Wang, S. Yin, *Small* **2024**, *20*, 2401386; e) J. Wang, H. Zhang, L. Yang, S. Zhang, X. Han, W. Hu, *Angew. Chem., Int. Ed.* **2024**, *63*, 202318149; f) B. Li, P. Ruan, X. Xu, Z. He, X. Zhu, L. Pan, Z. Peng, Y. Liu, P. Zhou, B. Lu, L. Dai, J. Zhou, *Nano-Micro Lett.* **2024**, *16*, 76; g) L. Li, Y. Tsang, D. Xiao, G. Zhu, C. Zhi, Q. Chen, *Nat. Commun.* **2022**, *13*, 2870.

[40] J. Fu, F. Hassan, J. Li, D. Lee, A. Ghannoum, G. Lui, M. Hoque, Z. Chen, *Adv. Mater.* **2016**, *28*, 6421.

[41] Y. Jiang, Y. Deng, R. Liang, J. Fu, D. Luo, G. Liu, J. Li, Z. Zhang, Y. Hu, Z. Chen, *Adv. Energy Mater.* **2019**, *9*, 1900911.

[42] T. Tam, S. Kang, M. Kim, S. Lee, S. Hur, J. Chung, W. Choi, *Adv. Energy Mater.* **2019**, *9*, 1900945.

[43] Y. Zhang, T. Hu, C. Ke, F. Han, W. Xiao, X. Yang, *Inorg. Chem. Front.* **2022**, *9*, 5774.

[44] C. Gu, X. Xie, Y. Liang, J. Li, H. Wang, K. Wang, J. Liu, M. Wang, Y. Zhang, M. Li, H. Kong, C. Liu, *Energy Environ. Sci.* **2021**, *14*, 4451.

[45] Z. Wu, H. Wang, P. Xiong, G. Li, T. Qiu, W. Gong, F. Zhao, C. Li, Q. Li, G. Wang, F. Geng, *Nano Lett.* **2020**, *20*, 2892.

[46] D. Ji, L. Fan, L. Li, S. Peng, D. Yu, J. Song, S. Ramakrishna, S. Guo, *Adv. Mater.* **2019**, *31*, 1808267.

[47] Q. Liu, Y. Wang, L. Dai, J. Yao, *Adv. Mater.* **2016**, *28*, 3000.

[48] a) S. Shinde, C. Lee, J. Yu, D. Kim, S. Lee, J. Lee, *ACS Nano* **2018**, *12*, 596; b) N. Wagh, D. Kim, C. Lee, S. Kim, H. Um, J. Kwon, S. Shinde, S. Lee, J. Lee, *Nanoscale Horiz.* **2023**, *8*, 921; c) N. Wagh, S. Shinde, C. Lee, S. Kim, D. Kim, H. Um, S. Lee, J. Lee, *Nano-Micro Lett.* **2022**, *14*, 190; d) N. Wagh, S. Shinde, C. Lee, J. Jung, D. Kim, S. Kim, C. Lin, S. Lee, J. Lee, *Appl. Catal. B* **2020**, *268*, 117746; e) S. Shinde, J. Yu, J. Song, Y. Nam, D. Kim, J. Lee, *Nanoscale Horiz.* **2017**, *2*, 333; f) M. Guo, L. Wang, Z. Huang, H. Li, T. Isimjan, X. Yang, *ACS Nano* **2024**, *18*, 17901; g) S. Das, A. Pathak, U. Phadikar, C. Kuila, A. Maji, T. Kuila, N. Murmu, R. Thapa, A. Kundu, *Adv. Funct. Mater.* **2024**, *34*, 2407078; h) A. Zhang, J. Yang, L. Yang, T. Yang, Y. Liu, L. Zhou, Z. Xu, X. Zhou, J. Tang, *Appl. Catal. B* **2024**, *359*, 124485; i) H. Wang, X. Niu, W. Liu, R. Yin, J. Dai, W. Guo, C. Kong, L. Ma, X. Ding, F. Wu, W. Shi, T. Deng, X. Cao, *Adv. Sci.* **2024**, *11*, 2403865; j) J. Zhang, X. Dong, G. Wang, J. Chen, R. Wang, *Appl. Catal. B* **2024**, *342*, 123459.

[49] C. Xia, L. Huang, D. Yan, A. Douka, W. Guo, K. Qi, B. Xia, *Adv. Funct. Mater.* **2021**, *31*, 2105021.

[50] Y. Dai, J. Yu, J. Wang, Z. Shao, D. Guan, Y. Huang, M. Ni, *Adv. Funct. Mater.* **2022**, *32*, 2111989.

[51] C. Lai, H. Li, Y. Sheng, M. Zhou, W. Wang, M. Gong, K. Wang, K. Jiang, *Adv. Sci.* **2022**, *9*, 2105925.

[52] M. Zhao, H. Liu, H. Zhang, W. Chen, H. Sun, Z. Wang, B. Zhang, L. Song, Y. Yang, C. Ma, Y. Han, W. Huang, *Energy Environ. Sci.* **2021**, *14*, 6455.

[53] Y. Guo, P. Yuan, J. Zhang, H. Xia, F. Cheng, M. Zhou, J. Li, Y. Qiao, S. Mu, Q. Xu, *Adv. Funct. Mater.* **2018**, *28*, 1805641.

[54] J. Liu, C. Zhao, D. Ren, J. Wang, R. Zhang, S. Wang, C. Zhao, B. Li, Q. Zhang, *Adv. Mater.* **2022**, *34*, 2109407.

[55] C. Z. Wang, M. Yu, W. Wang, *Appl. Catal. B* **2021**, *281*, 119514.

[56] N. Wagh, D. Kim, S. Kim, S. Shinde, J. Lee, *ACS Nano* **2021**, *15*, 14683.

[57] D. Lyu, S. Yao, A. Ali, Z. Tian, P. Tsiakaras, P. Shen, *Adv. Energy Mater.* **2021**, *11*, 2101249.

[58] F. Wang, O. Borodin, T. Gao, X. Fan, W. Sun, F. Han, A. Faraone, J. Dura, K. Xu, C. Wang, *Nat. Mater.* **2018**, *17*, 543.